Journal of Structural Geology 30 (2008) 1412–1428

Contents lists available at ScienceDirect

Journal of Structural Geology

journal homepage: www.elsevier.com/locate/jsg

Fabric superposition in upper mantle peridotite, Red Hills, New Zealand

Caroline E. Webber [a,*], Timothy Little [b], Julie Newman [c], Basil Tikoff [a]

[a] Department of Geology and Geophysics, University of Wisconsin-Madison, 1215 West Dayton Street, Madison, WI 53706, USA
[b] School of Earth Sciences, Victoria University of Wellington, Wellington, New Zealand
[c] Department of Geology and Geophysics, Texas A&M University, College Station, TX 77843, USA

ARTICLE INFO

Article history:
Received 27 June 2007
Received in revised form 20 July 2008
Accepted 1 August 2008
Available online 16 August 2008

Keywords:
Overprinting
Mantle
New Zealand
Anisotropy
Red Hills

ABSTRACT

At least four generations of superposed fabrics that formed at upper mantle conditions are recorded by field relations, mineral compositions, and olivine lattice preferred orientation in the Red Hills, an ultramafic massif in South Island, New Zealand. The oldest fabric is found in the Central Domain and contains north-dipping compositional bands of harzburgite, dunite, and minor lherzolite. Expressions of second-generation fabrics that cross-cut Central Domain fabric are cm-scale, south-dipping shear zones; and a >50 m-thick zone of south-dipping shear, the South-dipping Domain. A third, younger, superposed fabric occurs in a ≥1 km-thick package on the west side of the field area, called the West Domain. The West Domain is composed of harzburgite and lherzolite, and is characterized by steeply west-dipping foliation and by isoclinal folds of older compositional banding. The youngest fabric, the East Domain, is preserved in a ~50 m-thick zone on the east side of the field area. The East Domain is composed of lherzolite and contains cm-scale compositional bands that define a microstructually distinct, shallowly east-dipping foliation. The West and East Domains are interpreted to have formed by transposition of Central Domain fabric. Fabric transposition is generally expressed by an abrupt overprinting or truncation, rather than by a progressive deflection of foliations. This study demonstrates that multiple overprinting fabrics exist in the upper mantle, similar to the fabric superposition commonly observed in mid- to lower-crustal rocks.

© 2008 Elsevier Ltd. All rights reserved.

1. Introduction

The upper mantle is volumetrically a major component of the lithosphere, therefore understanding deformation in the upper mantle is critical to understanding large-scale, plate tectonic processes. The dominant source of information on mantle deformation comes from experimental deformation of olivine in laboratory settings (e.g., Kohlstedt and Goetze, 1974; Hanson and Spetzler, 1994; Wendt et al., 1998; Holtzman et al., 2003). Extrapolation from experimental to tectonic scales requires an assumption of deformational homogeneity; however, this may not be valid in naturally deformed rocks, depending on the scale of interest (Paterson, 2001). Shear wave splitting data in active tectonic settings is another source of insight on deformation in the lithospheric mantle (e.g., Savage, 2002 and references therein), but the technique requires averaging of physical properties over large regions. The direct measurement of mantle fabrics in exposed ultramafic bodies is one method to assess fabric homogeneity and to correlate between these different spatial scales of observation.

A variety of field studies in outcrops of the lithospheric mantle have investigated fabrics at the intermediate (100 m to km) scale. Well-known areas include Oman (e.g., Michibayashi and Mainprice, 2004), the Pyrenees (e.g., Vissers et al., 1997), Newfoundland (e.g., Suhr, 1992), and the western Mediterranean (e.g., Van der Wal and Vissers, 1993; Dijkstra et al., 2004). Commonly, mantle deformation fabrics are interpreted as forming at a spreading center. For example, Suhr (1992) reported multiple overprinting fabrics in the Bay of Islands Ophiolite, and interpreted the fabrics as forming at a spreading center. Other examples of mantle shear zones are interpreted in the context of uplift and emplacement of an ultramafic massif. Well-known examples of this type of deformation come from Alpine peridotites, specifically, the Pyrenees (e.g., Vissers et al., 1997) and Greece (e.g., Dijkstra et al., 2004).

Our study of the Red Hills massif, South Island, New Zealand focuses on a polyphase history of deformation that took place in upper mantle rocks at inferred upper mantle pressure and temperature conditions. Detailed geologic mapping in Red Hills reveals that fabric transposition occurred on at least two scales, and we identify at least three superposed zones of localized deformation. A Central Domain of lithologically heterogeneous and

* Corresponding author. Present address: ExxonMobil Production Company, 396 West Greens Road, CORP-WGR-408, Houston, TX 77067, USA. Tel.: +1 608 469 4413; fax: +1 713 431 1570.
E-mail address: carolinewebber581@hotmail.com (C.E. Webber).

0191-8141/$ – see front matter © 2008 Elsevier Ltd. All rights reserved.
doi:10.1016/j.jsg.2008.08.002

compositionally banded ultramafic rock is overprinted by distinctive fabrics in its center and on its western and southeastern flanks. This type of fabric superposition is commonly observed in mid- to lower-crustal rocks, but is rarely reported for the lithospheric mantle. This study focuses on the field documentation of these patterns and considers the implications of compositional and structural heterogeneity for upper mantle deformation.

2. Tectonic setting and geologic history

2.1. Geologic setting of the Dun Mountain Ophiolite Belt

The Red Hills ultramafic massif ($\sim$100 km^2) is located in the northern portion of South Island, New Zealand (Fig. 1A). The Red Hills massif is part of the Dun Mountain Ophiolite Belt (DMOB), a package of ultramafic rocks and associated sediments that is discontinuously exposed for >1100 km. The DMOB is divided into two segments dextrally offset by $\sim$460 km on the Alpine Fault. The DMOB is up to $\sim$8 km wide (Davis et al., 1980) and gravity surveys indicate that the ultramafic part of this body is <4 km thick (Malahoff, 1965).

The DMOB is part of the Dun Mountain-Maitai Terrane, which also includes mafic rocks of the Lee River Group, sedimentary rocks of the Maitai Group, and the Patuki and Croisilles Mélanges (Fig. 1B) (Davis et al., 1980; Johnston, 1986; Kimborough et al., 1992). Ultramafic rocks of the DMOB are separated by faults from the remainder of the mafic and sedimentary rocks in the Dun Mountain-Maitai Terrane. The Brook Street Terrane, which is composed of volcanics and volcaniclastics, is locally in fault contact with the western margin of the Dun Mountain-Maitai Terrane (Johnston, 1986). The eastern margin of the Dun Mountain-Maitai Terrane is in fault contact with accreted sedimentary rocks of the Pelorus Group and the Marlborough Schist (Johnston, 1986).

The DMOB is interpreted to have formed 280 $\pm$ 5 Ma, based on U/Pb ages obtained from plagiogranite dikes located in the DMOB (Kimborough et al., 1992). The age of emplacement of the Dun Mountain-Maitai Terrane is unknown, but previous workers suggest a late Permian emplacement, prior to folding and metamorphism associated with the Jurassic – Early Cretaceous Rangitata Orogeny (Johnston, 1982; Davis et al., 1980). Offset of the ultramafic body along the Alpine Fault has occurred since $\sim$25 Ma (Sutherland, 1995; Cooper et al., 1987).

2.2. Origin of the Dun Mountain Ophiolite Belt

The tectonic setting for the formation of the DMOB is unknown. Prior to recognition of ophiolites as obducted oceanic crust, Challis (1965) and Walcott (1965) suggested an intrusive origin. Based on major and minor element chemistry of the ultramafic rocks, Davis et al. (1980) proposed that the DMOB was formed at a mid-ocean ridge. Coombs et al. (1976) suggested that the Dun Mountain ultramafics formed at a spreading center adjacent to an island arc (i.e. the Brook Street Terrane). Based on major and trace element chemistry of basaltic dikes in the Red Hills massif and associated Lee River Group, Sano et al. (1997) suggested that the Red Hills was generated at a spreading center in a back-arc basin. On the basis of similar types of data, Sivell and McCulloch (2000) also argued that the Dun Mountain Ophiolite formed in a supra-subduction zone environment (but probably in a forearc to proto-island arc setting).

2.3. Previous work in the Red Hills ultramafic massif

The Red Hills are mostly unserpentinized, and provide significant horizontal exposure ($\sim$100 km^2) and vertical relief (>700 m). Walcott (1965) conducted the first structural study of the Red Hills massif, and mapped (1:50,000) a region of $\sim$260 km^2 including the Red Hills and adjacent areas. Walcott (1965, 1969) divided the

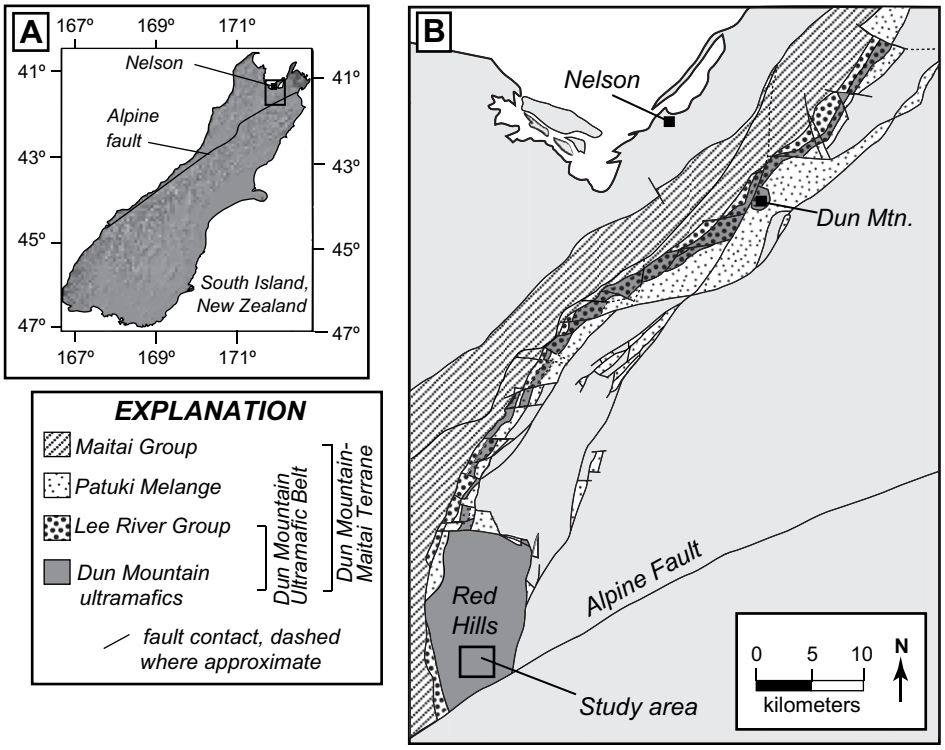

Fig. 1. Location of Red Hills study area. (A) Digital elevation model (digital data available free from www.geographix.co.nz) of South Island, New Zealand illustrating location of Alpine Fault. Box denotes area of image in part B. (B) Map of the northern segment of the Dun Mountain Ophiolite Belt. Note location of Red Hills ultramafic massif and the study area.

ultramafic rocks into two domains: (1) a basal zone, consisting of non-foliated harzburgite with a "proto-clastic" (i.e. ductilely deformed) texture; and (2) an upper zone, composed of foliated dunite, harzburgite, and gabbro containing abundant dikes and displaying a xenomorphic-granular texture. Within the upper zone, Walcott (1965) identified two fabrics, and noted that a zone of south-dipping foliation cut the pre-existing, north-dipping compositional foliation at Porter's Knob. Based on the orientation of compositional foliation, Walcott (1965) interpreted Red Hills massif as an antiform with Porter's Knob located in the hinge.

2.4. Present study of the Red Hills massif

We mapped a portion ($\sim$2 km^2) of the Red Hills massif near Porter's Knob to better understand the history of mantle deformation in this location. We specifically chose to locate our study at Porter's Knob, because this area was interpreted as the hinge of a regional antiform by Walcott (1965) and Christensen (1984).

In this paper, we present data on both km-scale and cm-scale structures, and show that these structures formed at temperatures consistent with upper mantle conditions. These data support the conclusion that the Red Hills is not a massif-scale fold, but has been subject to several penetrative phases of fabric superposition at the micro- to outcrop-scale.

3. Rock types

The Porter's Knob field area includes: $\sim$60% lherzolite, $\sim$40% harzburgite, and $<$1% dunite. Harzburgite crops out in the central portion of the field area forming a zone $\sim$800 m wide. Dunite bodies that are 100–500 m^2 crop out in areas that are otherwise compositionally dominated by harzburgite and lherzolite. Contacts between harzburgite and lherzolite are transitional over $\sim$10–20 m. Contacts between dunite and harzburgite or lherzolite are transitional over $\sim$1–3 m.

Clinopyroxenite, orthopyroxenite, and olivine websterite dikes that are 1–15 cm thick cross-cut host rock composed of lherzolite, harzburgite, and dunite. These dikes crop out throughout the Red Hills field area. Diabase dikes that are 1–2 m thick cross-cut all other lithologies.

In the following section, we describe the modal composition and mesoscopic heterogeneity evident in host and dike rock lithologies. Additionally, we describe the outcrop patterns of each rock type.

3.1. Lherzolite

Lherzolite contains 65–75% olivine, 17–27% orthopyroxene, 6–7% clinopyroxene and $<$1% spinel. Where locally present, plagioclase ($<$5%) occurs in discontinuous, thin layers that are typically one or two grains thick. Lherzolite also contains some alternating, 1–10 cm thick, compositional layers of dunite and harzburgite. Lherzolite is easily distinguished in the field because of its dark brown color on weathered surfaces, and its abundant clinopyroxene dikes (these are 1–10 cm thick and folded). Lherzolite outcrops on both the eastern and western margins of the field area, although it is also rarely found within the central section.

3.2. Harzburgite

Harzburgite contains 66–85% olivine, 13–31% orthopyroxene, $<$5% clinopyroxene, and $<$1% spinel. Some samples of harzburgite contain plagioclase (1%). The harzburgite occurs in two types: (1) olivine-rich harzburgite, which contains $>$30% dunite layers, and (2) olivine-poor harzburgite, which contains $<$30% dunite layers. Both olivine-rich and olivine-poor harzburgite contain alternating compositional layers of dunite and harzburgite that range in thickness from 1–2 cm thick (central portion of the field area) to 6–10 cm thick (western portion of the field area). Olivine-rich harzburgite is primarily concentrated in the western part of the field area, whereas olivine-poor harzburgite is concentrated in the central portion.

3.3. Dunite

Dunite bodies contain 98% olivine, 1% spinel, and minor amounts of clinopyroxene and orthopyroxene ($<$1%). Dunite bodies crop out in three different forms, including: (1) tabular bodies (2–10 cm) with gradational contacts that alternate with pyroxene-rich bands and contribute to the compositional foliation (Fig. 2A); (2) tabular bodies (2–150 cm) with sharp contacts that discordantly cross-cut host rock foliation (Fig. 2B); and (3) large irregularly shaped bodies (50–500 m^2) that have gradational contacts with host rock (Fig. 2C). Dunite bodies that are concordant and discordant to compositional foliation are petrologically similar. Both commonly contain thin zones of clinopyroxene that mark the contact between the dunite bodies and the host rock. In two examples within the field area, tabular dunite bodies that cross-cut compositional foliation are observed to grade into clinopyroxenite bodies along strike.

Irregularly shaped dunite bodies display an intertonguing contact with host rock in a zone 1–2 m wide. Compositional foliation was not apparent in these dunite bodies, thus it is not obvious whether fabrics in the adjacent harzburgite and lherzolite are continuous in dunite bodies. Large dunite bodies typically contain abundant pyroxene-rich dikes and spinel pods.

3.4. Pyroxene-rich dikes

Dikes composed of orthopyroxenite, clinopyroxenite and olivine websterite cross-cut harzburgite, lherzolite, and dunite host rock. Some olivine websterite and clinopyroxenite dikes contain plagioclase. Dikes typically range in thickness from 1 to 15 cm, but one population of clinopyroxenite dikes is distinctive because these dikes are $\leq$1 cm thick and dikes have sharp contacts with the host rock. Contacts between other pyroxene-rich dikes and host rock are commonly poorly defined in outcrop, with cm-scale intertonguing of dike rock and host rock. Contacts are also poorly defined in thin section, where the larger grain size and different lithology of the dikes is the most distinctive difference between dike and host rock. No variation in grain size was observed from the dike margins to their centers.

3.5. Diabase dikes

Diabase dikes are $\sim$1–2 m thick, can be mapped for 10–100 m and cross-cut all other rock types. Host-dike contacts are sharp, but typically are poorly preserved because of serpentinization at the dike–host margin. Diabase dikes strike NNW and dip steeply to subvertically. The composition of the dikes is $\sim$63% clinopyroxene, 33% plagioclase, and 2% spinel. They also contain minor amounts ($<$1%) of olivine, orthopyroxene, prehnite, or quartz.

4. Kilometer-scale structural domains

Rock types in the Red Hills field area show a complicated map pattern, and the contacts between adjacent rock types are typically poorly exposed. Although harzburgite is the dominant rock type in the central portion of the field area and lherzolite is dominant on the eastern and western margins, there is significant variation in rock type on the decimeter scale.

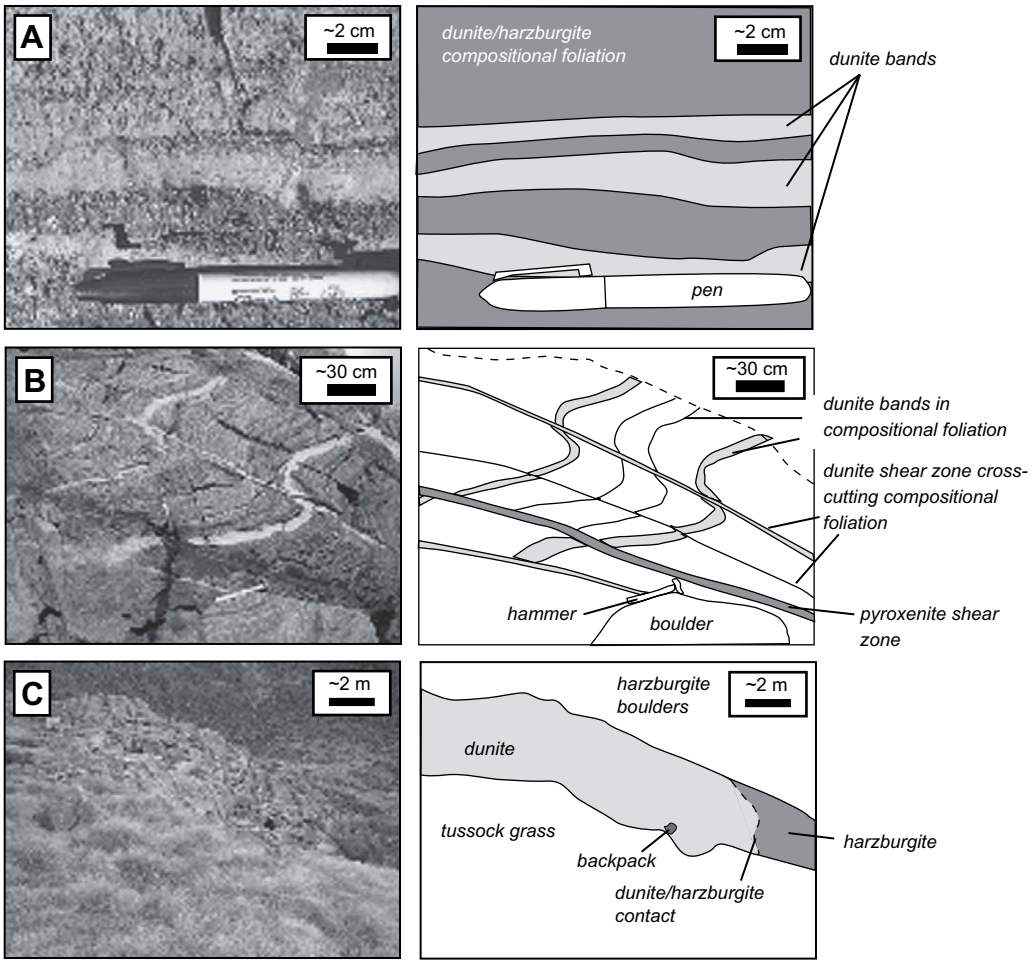

Fig. 2. Dunite occurrences in the Red Hills field area. (A) Image and sketch of compositional foliation illustrating alternating dunite and harzburgite bands at the hand sample scale. (B) Image and sketch of outcrop located at Porter's Knob (Central Domain, Fig. 3), illustrating compositional foliation and cross-cutting, south-dipping, dunite and pyroxenite shear zones. (C) Irregularly shaped, relatively large-scale (~500 m^2) dunite body in contact with harzburgite.

In contrast, styles of structural deformation show a clear map pattern, allowing the region to be divided into four structural domains (Fig. 3). The domains are defined on the basis of mesoscopic foliation characteristics, i.e. thickness of bands forming a compositional foliation, the type of folding of compositional foliation, and the orientation of foliation. Based on these characteristics, we defined the following structural domains and named them for their geographic position in the field area: Central Domain, West Domain and East Domain. An additional domain, the South-dipping Domain, occurs as a thin enclave in the Central Domain and is named for the orientation of foliation it contains.

4.1. Central Domain

4.1.1. Host rock

The central portion of the field area (~2 km × ~1 km) is characterized by a north-dipping compositional foliation. Harzburgite is the dominant rock type in the Central Domain (~90%), although lherzolite and dunite are also present. The mesoscopic characteristics of compositional foliation are similar in harzburgite and lherzolite. No compositional foliation was observed in irregularly shaped bodies of dunite.

Harzburgite and lherzolite in the Central Domain contain a north-dipping compositional foliation defined by alternating 2–3 cm-wide bands that are relatively olivine-rich (>90% olivine) or olivine-poor (<90% olivine) (Fig. 2A and B). Compositional foliation is typically folded by small amplitude (≤10 cm) open folds. A foliation defined by the preferred dimensional alignment of abundant elongate spinels and pyroxenes is observed to be parallel to the compositional layering throughout this domain. Elongate, preferentially oriented spinel or orthopyroxene, or elongate aggregates of spinel define a lineation in compositional layers. The mean orientation of foliation is 277 50°N, in which the lineation plunges shallowly to the E or W (Fig. 4A). In some lherzolite outcrops, a foliation is also defined by plagioclase mineral elongation. Small-scale, south-dipping shear zones that are composed of dunite, pyroxenite, or olivine websterite cross-cut and offset the compositional foliation in the Central Domain (Figs. 2B and 4B). The rocks that exhibit Central Domain compositional foliation will be referred to as Central Domain host rocks throughout the remainder of this paper.

4.1.2. Pyroxene-rich dikes in the Central Domain

Dikes composed of orthopyroxenite, clinopyroxenite and olivine websterite range in thickness from <1 to ~10 cm. Pyroxenite and olivine websterite dikes are observed in a variety of orientations in the Central Domain (Fig. 4C). Some dikes are folded or boudinaged. Although cross-cutting relationships indicate several generations of diking, there are no clear relationships between dike composition or orientation and age of intrusion.

4.1.3. Cross-cutting, cm-scale shear zones in the Central Domain

A series of cm-scale shear zones was documented by Walcott (1965) and are a unique feature of the Red Hills area. Dunite, pyroxenite, and olivine websterite shear zones cut and offset

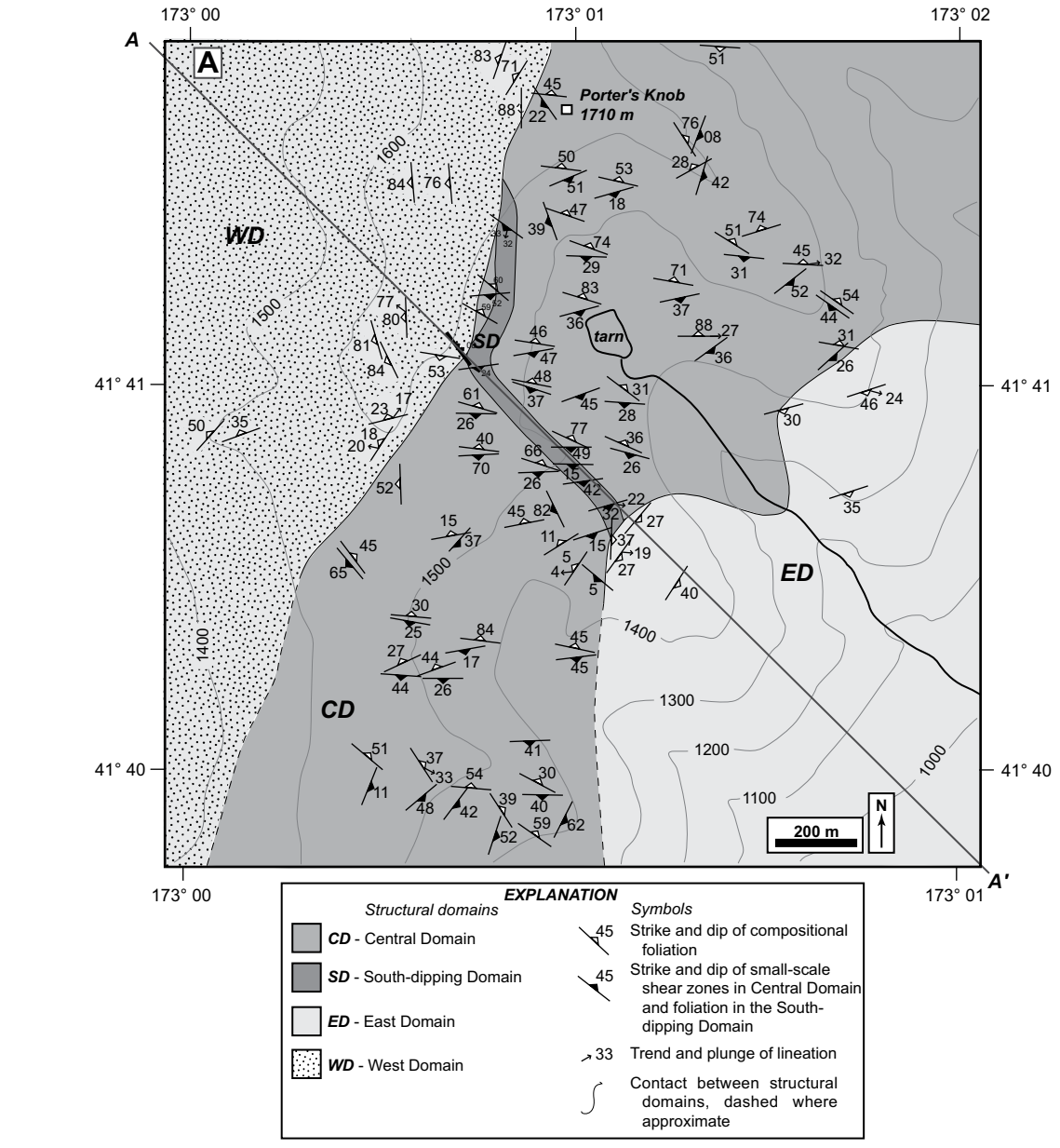

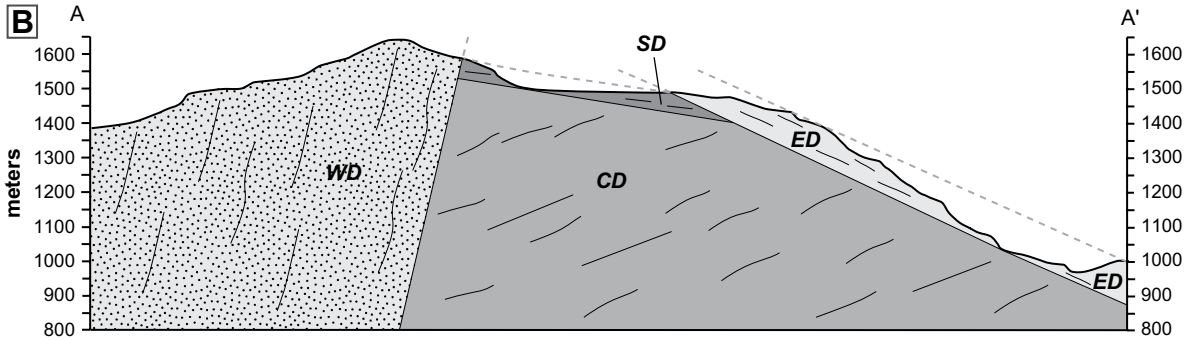

Fig. 3. (A) Structural domain map of the Red Hills study area. (B) Cross-section A–A′.

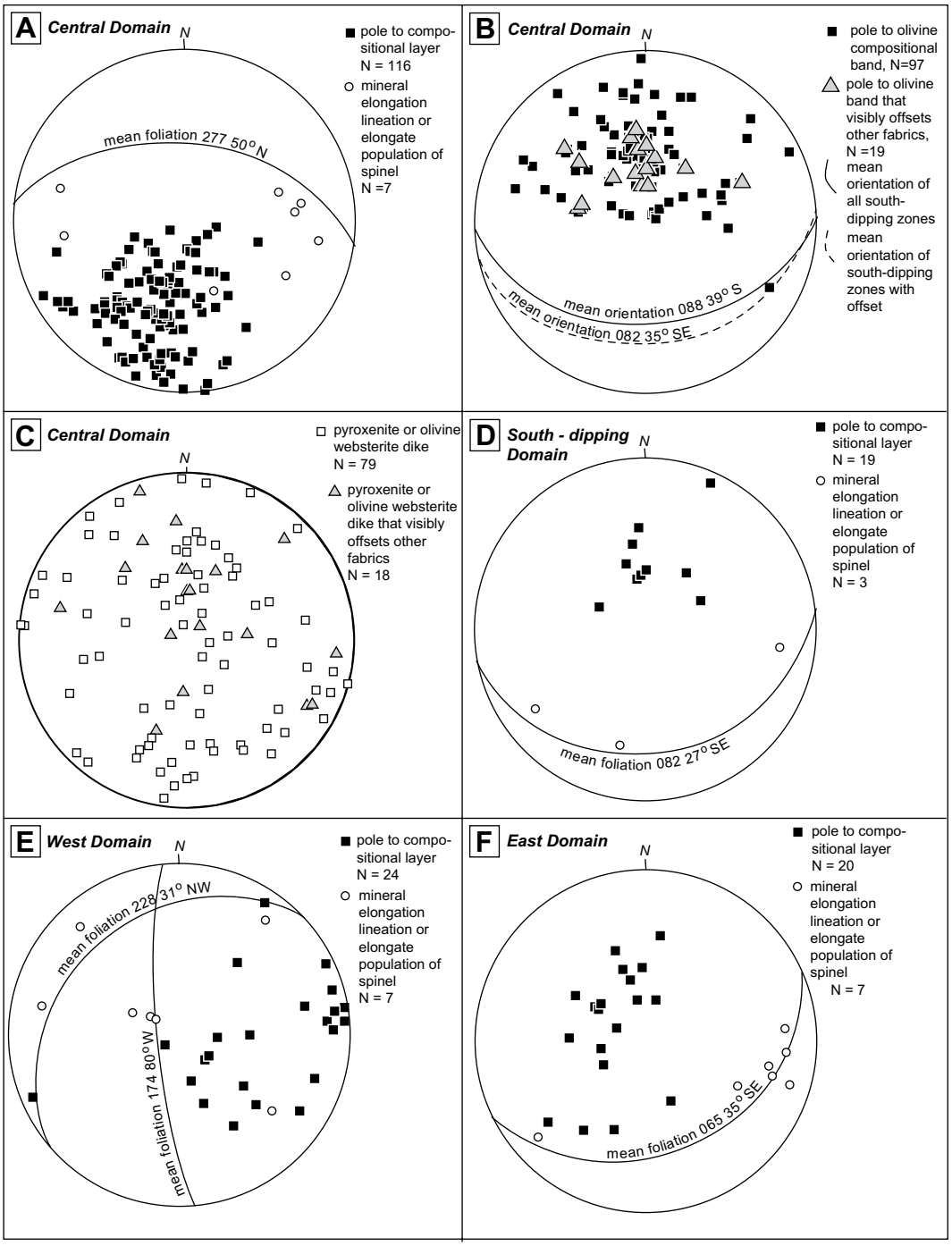

Fig. 4. Lower hemisphere equal area nets showing the orientations of structural features in the study area. (A) Orientation of compositional foliation and lineation in the Central Domain. (B) Orientation of south-dipping dunite, pyroxenite, and olivine websterite shear zones and a population of those shear zones that contain visible offset in the Central Domain. (C) Orientation of pyroxenite and olivine websterite dikes in the Central Domain and the population of those dikes that contain visible offset. Parts (D), (E), and (F) show the orientation of compositional foliation and lineation in the South-dipping Domain (D), West Domain (E), and East Domain (F).

compositional foliation and older dikes throughout the Central Domain (Figs. 2B and 4B). These cross-cutting shear zones are consistent in orientation, but heterogeneous with respect to size, composition, and amount of offset. The shear zones primarily strike E–W (±~30°) and dip gently to moderately S. They range in thickness from <1 to ~50 cm and are primarily composed of dunite. Some (<25%) are composed of clinopyroxenite, orthopyroxenite, or olivine websterite. The amount of offset (2–90 cm) on cm-scale shear zones is measured from offset dikes or distinct bands of compositional foliation in the host rock. Both normal and reverse offsets are observed.

Foliation and lineation in the south-dipping shear zones are difficult to discern in outcrop because foliation planes are almost never exposed as a 2D surface. Where measured in thin section, foliation is defined by elongate aggregates of spinel that strike E–SE and dip moderately S–SW. Where measured in outcrop, lineation plunges approximately down-dip (S).

Fig. 5 shows one shear zone that is particularly informative on timing of small-scale shear zone deformation. A folded orthopyroxenite dike is offset in a reverse, top-to-the-north, sense by the shear zone. The orthopyroxenite dike is also boudinaged within the shear zone. This relationship is consistent with the following

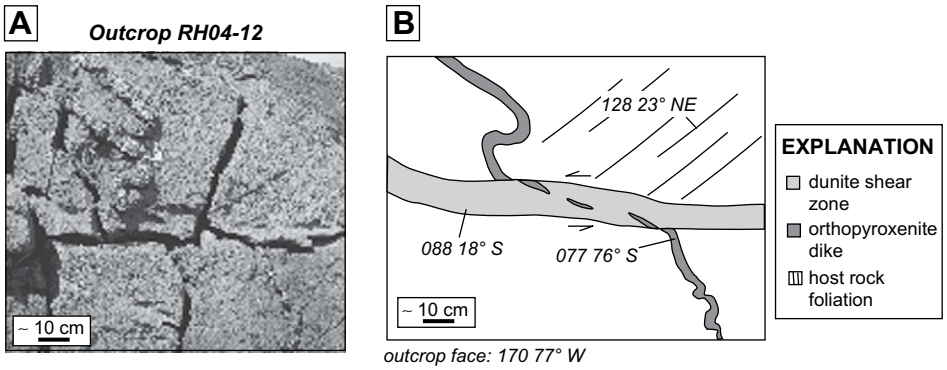

Fig. 5. Example of a small-scale shear zone at outcrop RH04-12 (Central Domain). (A) Outcrop photo. (B) Sketch of outcrop.

geologic history: (1) a tabular south-dipping dunite band was cross-cut by an orthopyroxenite dike; (2) the orthopyroxenite dike was folded; and, (3) the tabular dunite body was activated as a shear zone which offset and boudinaged the orthopyroxenite dike in a reverse sense.

More details about the field aspects of these shear zones, in addition to detailed microstructural information, are given in Webber (2005) and Webber et al. (submitted for publication).

4.2. South-dipping Domain

The ~50 m-thick South-dipping Domain is entirely contained within the Central Domain and is composed of harzburgite. It crops out near Porter's Knob and is exposed for ~1 km in a zone that strikes EW and dips ~15° south (Fig. 3). Foliation in the South-dipping Domain is similar in appearance to compositional foliation in the Central Domain, and has a mean orientation of 082 27° SE (Fig. 4D). Deformed aggregates of spinel grains (~200–500 μm) define a foliation that is sub-parallel to the compositional foliation, and an elongation lineation. Additionally, orthopyroxene has a shape-preferred orientation that is parallel to the orientation of spinel and compositional foliation.

The South-dipping Domain contains shear zones of dunite, pyroxenite, and olivine websterite, all of which dip southward. Unlike in the Central Domain, determining offset on small-scale shear zones in the South-dipping Domain is difficult, because the shear zones cross-cut host rock lithologies at low angles (Fig. 6A). The South-dipping Domain also contains pyroxenite and olivine websterite dikes, which are similar in composition and thickness to dikes observed in the Central Domain. Dikes in the South-dipping Domain are commonly folded with axial planes parallel to the dominant foliation in this domain.

The South-dipping Domain is observed in contact with the Central Domain at two locations ~40 m below Porter's Knob (east side). At these locations, we identify a progression of north-dipping compositional banding that grades into a transitional foliation defined by both north-dipping and south-dipping banding and finally into a foliation defined by dominantly south-dipping compositional bands in the strongly deformed interior of the South-dipping Domain. The transition from north-dipping to south-dipping compositional foliation occurs over a distance of ~10 m.

4.3. West Domain

Foliation in the West Domain (≥2 km long and ≥1 km thick) is defined in two different ways (Fig. 6B and C). Foliation in harzburgite is defined by irregularly shaped olivine- or pyroxene-rich domains and elongate pods that range in thickness from ~6 to 10 cm and are commonly tightly to isoclinally folded. Fold axial planes are sub-parallel to the compositional foliation in the West Domain. Foliation in lherzolite is defined by discontinuous, planar clinopyroxenite bands (≤1 cm thick); abundant tightly to isoclinally folded clinopyroxenite dikes; and planar or isoclinally folded olivine-rich bands (~1–3 cm thick). Spinel grains (~200–500 μm) express a preferred dimensional alignment that is sub-parallel to the compositional foliation and also define an elongation lineation (Fig. 4E). Additionally, olivine grains exhibit a well-defined grain shape-preferred orientation that parallels the orientation of spinel.

Foliation occurs in two orientation modes that are not related to rock type (Fig. 4E). One foliation population strikes ~N–S and dips steeply to the east or to the west. Foliation in this orientation is primarily concentrated on the NE side of the domain. Another population strikes NE–SW and dips moderately to the NW. This foliation is concentrated on the SW side of the domain.

The contact between West and Central Domains is well exposed ~100 m NE of Porter's Knob. At this location, we observe a transition in the thickness and folding style of compositional layers. Several meters west of the transition in foliation characteristics, we observe a change in foliation orientation. The transition zone is ~10 m thick.

A north-dipping compositional foliation, identical in orientation and character to that observed in the Central Domain, is locally preserved in two ~2 m^2 locations in the West Domain. Field relations suggest that these fabrics are locally preserved sections of the Central Domain, which were overprinted by the West Domain fabric. The preservation of the Central Domain fabric, in the same orientation as observed in the Central Domain, suggests that fabric transposition does not result in progressive deflection of foliation. Rather, fabric transposition is expressed by an abrupt truncation and discrete overprinting of fabrics.

4.4. East Domain

The ~50 m thick East Domain is distinguished from the other structural domains by a planar fabric that dips 15–30° ESE (Fig. 4F). The fabric is defined by irregularly spaced, planar, 1–3 cm thick olivine-rich or pyroxene-rich bands; planar pyroxene-rich dikes that are 1–10 cm thick; and planar plagioclase-rich bands that are <1 cm thick (Fig. 6D). The East Domain contains a foliation that is reinforced by planar concentrations of spinel that are sub-parallel to the main compositional foliation. Within this foliation, a lineation is defined by an elongate preferred dimensional alignment of deformed aggregates of spinel. Lherzolite is the dominant rock type in the East Domain. The only compositional variation we observe in the East Domain is one 5 m^2 dunite body. In the dunite, the East Domain foliation is defined by grain shape-preferred orientation of spinel.

The East Domain is in contact with the Central and South-dipping Domains on an E–W-trending ridge south of Porter's Knob

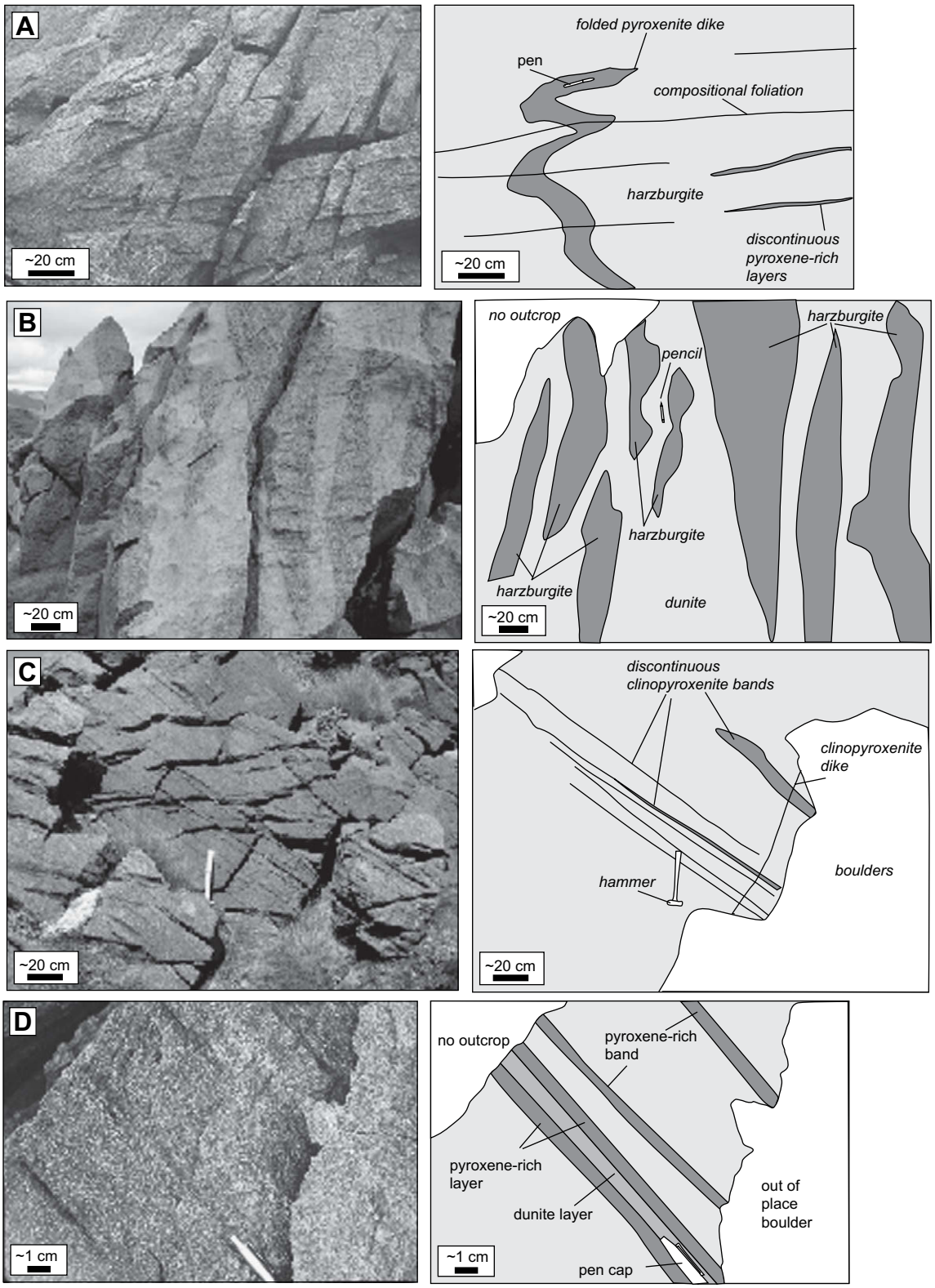

Fig. 6. Field photographs and sketches of compositional foliation in the South-dipping, West, and East Domains. (A) Photo and sketch of harzburgite deformed in the South-dipping domain. Note folded dike with axial planes parallel to compositional foliation. (B) Harzburgite deformed in the West Domain, showing a foliation defined by irregularly shaped harzburgite and dunite bands. (C) Lherzolite deformed in the West Domain, showing a foliation defined by discontinuous clinopyroxenite bands. (D) Lherzolite deformed in the East Domain. Note the foliation defined by planar, thin compositional layers.

and at another E–W-trending ridge east of Porter's Knob. At both sites, we observe a gradual change (~10 m) in the dominant rock type from harzburgite grading into lherzolite to the southeast. Farther east of the lithologic change, we observe a change in foliation type occurring over a distance of <10 m. The change to East Domain is easily identified by its planar compositional foliation and foliation orientation.

4.5. Late-stage faulting

Two types of young brittle faults occur in the Red Hills field area: (1) faults marked by meter-wide zones of breccia, and (2) faults marked by meter-wide serpentine zones. Poorly cemented breccias crop out in several locations in the West Domain as boulders or discontinuous bands that are observed for ≤10 m and strike ~150°. The breccia is composed of dunite, harzburgite, or lherzolite clasts that are ≤10 cm in diameter. Minor amounts of serpentine are associated with breccia zones. We interpret these breccia zones to mark locations of brittle faults. Displacement on the faults is unknown, as contacts with host rock are not exposed and no offset markers were observed.

Serpentine-rich zones that are 1–2 m wide located in the Central, East, and West Domains crop out as topographic depressions. East of Porter's Knob, several serpentine zones are observed to strike N–S, but one serpentine zone south of Porter's Knob strikes NW–SE. The dip of these zones is unknown, as they are not well exposed in three dimensions. Offset on these faults is unknown.

5. Microstructures in structural domains

5.1. Host rock microstructures of the Central, South-dipping, and West Domains

Host rock microstructures of the Central, South-dipping, and West Domains are similar and are characterized by a bimodal distribution of large, elongate strained grains and small, minimally strained grains (porphyroclastic texture; Mercier and Nicolas, 1975). Microstructures are different in each mineral (Fig. 7A). Olivine exhibits 120° triple junctions, grain boundaries are typically straight to slightly curvilinear, and olivine grain shapes are moderately flattened (e.g., 7 mm:4 mm). Larger olivine grains contain sharp kink-band boundaries and smaller, recrystallized grains. Orthopyroxene grains are irregularly shaped or slightly elongate and range up to ~3 mm, but most are 1–2 mm in diameter. Commonly, orthopyroxene contains ≤5 μm wide clinopyroxene exsolution lamellae and some samples contain ≤1 μm wide spinel exsolution lamellae. Such lamellae are a characteristic microstructure in orthopyroxene throughout the study area. Orthopyroxene has a poikioblastic texture; it contains abundant inclusions of olivine (≤1 mm in diameter) or partially enclosed olivine blebs. Clinopyroxene is irregularly shaped and is ~0.5–1 mm in diameter. Spinel typically

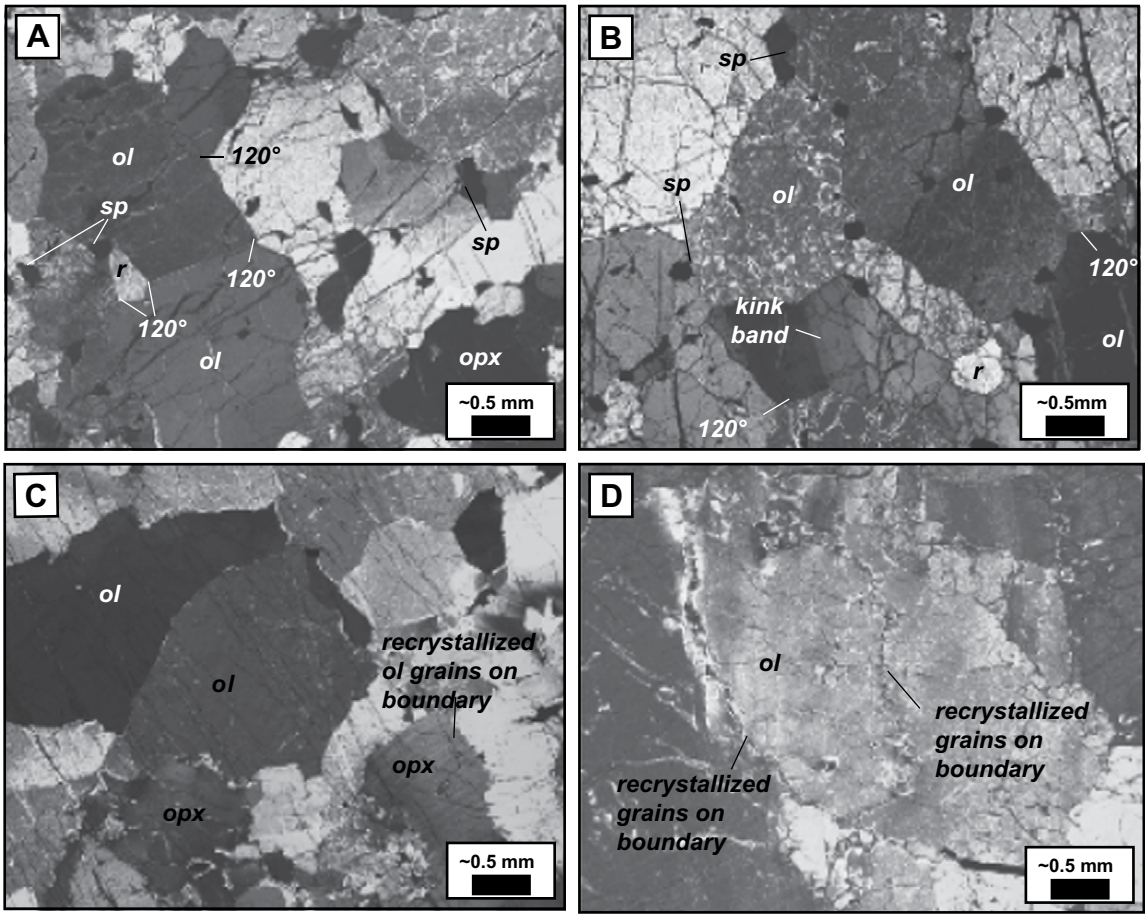

Fig. 7. Photomicrographs taken with crossed polars illustrating microstructures in each structural domain. All images are parallel to lineation and perpendicular to foliation. Olivine is indicated by the symbol "ol," orthopyroxene is indicated by "opx," spinel is indicated by "sp," and recrystallized grains are denoted as "r." (A) Central Domain harzburgite; 120° triple junctions and several smaller (recrystallized) grains. (B) Dunitic small-scale shear zone cross-cutting compositional foliation in the Central Domain. Note that grain size and microstructures are similar to host rock shown in A. (C) East Domain, lherzolite. Note the curved grain boundaries. (D) East Domain, dunite. Note the small (recrystallized) grains surrounding the large olivine grains. See text for further explanation.

occurs as inclusions in olivine grains or as deformed lenticular aggregates displaying a distinct grain shape-preferred orientation that is parallel to compositional foliation.

Microstructures are similar in harzburgite, lherzolite, and dunite. Grain size, however, is typically the smallest in lherzolite and largest in dunite ($\leq$10 mm). In some lherzolites, plagioclase occurs as $\sim$1 mm long grains with curved grain boundaries and is located in foliation-parallel bands that are $<$5 mm wide.

5.2. Microstructures in small-scale shear zones in the Central Domain

Microstructures in the small-scale shear zones of the Central Domain are similar to those observed in Central Domain host rock. Additionally, there are no consistent differences in grain size between the south-dipping zones and the surrounding host rocks; the grain size in any specific shear zone is slightly larger or smaller than the adjacent host rock. There is no significant grain size reduction, characteristic of mylonites, in these shear zones.

In dunite shear zones, olivine microstructures include 120° triple junctions, abrupt or patchy undulose extinction, deformation bands, and grain boundaries that are straight to slightly curved (Fig. 7B). Equant to slightly elongate recrystallized grains are abundant, and grain boundary contacts between olivine hosts and recrystallized grains are commonly serrate. Olivines range from equant $\sim$1 mm grain to elongate grains $\sim$6 mm long. A few dunite shear zones also contain orthopyroxene. Where present, orthopyroxene is $\sim$1–3 mm in diameter, irregularly shaped, contains clinopyroxene exsolution lamallae, and commonly encloses blebs of olivine. Spinel grains are equidimensional to slightly elongate and range in size from $\sim$100 to 300 μm.

Pyroxene grain size is a primary microstructural difference between dunite and pyroxene-rich shear zones. In clinopyroxenite shear zones, clinopyroxene grains are typically $\leq$10 mm in diameter and are equant to elongate (3:1 aspect ratio). Orthopyroxenes are typically equant and 2–5 mm in diameter in orthopyroxenite shear zones. In olivine websterite shear zones, both pyroxenes are equant and 1–2 mm in diameter. In pyroxene-rich shear zones, pyroxenes typically have abundant exsolution lamellae of orthopyroxene or clinopyroxene and exhibit patchy undulose extinction or kink bands. Contacts between pyroxene and olivine grains are typically curved, whereas grain boundaries between pyroxene grains are straight or serrate. Few spinel grains are present; where observed, they are round, $\sim$2 mm in diameter, and contain blebs of olivine.

5.3. Microstructures in the East Domain

The East Domain microstructures are distinct from those of other structural domains in the Red Hills field area. Grain boundaries are highly curvilinear to interlobate and lack well-developed 120° triple junctions. Many olivine grains have a core-and-mantle structure. Furthermore, olivine grains in East Domain samples do not contain a well-developed grain shape-preferred orientation, a dominant fabric element in other domains.

Microstructures are similar in lherzolite and dunite, except that the mean grain size is larger in dunite ($\leq$15 mm) than in lherzolite (2–5 mm) (Fig. 7C and D). In both rock types, olivine grains are equant to slightly elongate and have a bimodal distribution. Olivine grains that are $<$0.5 mm in diameter mantle larger olivine grains that are 2–15 mm in diameter. Grain boundaries between adjacent olivine grains or between olivine and orthopyroxene are curvilinear to interlobate, and, in some cases, serrate. Olivine grains exhibit patchy to sweeping undulose extinction, and contain deformation bands in some samples. Orthopyroxene and clinopyroxene grains are typically equant or irregularly shaped and range in size from $\sim$2 to 3 mm (orthopyroxene) or $\sim$1 mm in diameter (clinopyroxene). Orthopyroxene and clinopyroxene contain pyroxene exsolution lamellae, and in some samples spinel exsolution lamellae. Plagioclase occurs as round or irregularly shaped grains ($\leq$1 mm) in some lherzolites. Spinel grains are $\sim$200–400 μm in diameter and are typically blocky or irregularly shaped.

6. Olivine lattice preferred orientation (LPO)

6.1. Olivine LPO method

We measured olivine LPOs in samples of host rock on a universal stage microscope. In the following section, we present the results of these measurements from three representative samples in the Central Domain, and one representative sample from the South-dipping, West, and East Domains. In each sample, we measured $\geq$100 olivine grains. Data are plotted in two different ways (Fig. 8). First, the olivine axes were rotated such that the host rock foliation for each outcrop strikes E–W and dips vertically, and lineation is horizontal in the plane of foliation (Fig. 8; "sample-specific reference frame"). All data is first discussed with respect to this standard reference plane. Second, the olivine axes are plotted in real coordinate space, to allow the reader to compare the spatial orientation of the fabrics ("geographic reference frame"). This latter reference frame is essential to understanding the overprinting relations.

6.2. Results: olivine LPO of structural domains

In Central Domain host rock, olivine [100] axes are approximately coincident with the plane of foliation (sample 12D, Fig. 8) but may be up $\sim$30° from the lineation (sample 9B; Fig. 8). The [010] axes form a maximum sub-perpendicular to foliation, and the [001] axes form a maximum in the plane of foliation sub-perpendicular to lineation.

The olivine LPO of small-scale south-dipping shear zones that cross-cut Central Domain host rock are complex. When viewed with respect to the sample-specific reference frame, the LPO data for the south-dipping shear zones seem discordant to those in the enclosing host rocks (sample 12A, left-hand side of Fig. 8). In the geographic reference frame, however, this discordance is absent (upper right-hand side of Fig. 8, compare samples 9B, 12D, and 12A). From this we infer that the shear zone LPO retains evidence for the dominant LPO of the host rock. However, these LPO data suggest that the Central Domain has been variably overprinted by the later deformation in the small-scale shear zones and South-dipping, West, and East Domains. These LPO fabrics in the small-scale shear zones are explicitly addressed in another paper (Webber et al., submitted for publication).

The olivine LPO data measured in the South-dipping Domain are distinct from that in the Central Domain and yield a pattern of double maxima for [100] and [001] axes and a weak girdle distribution of [010] axes. The [100] axes form one maximum that is parallel to foliation and perpendicular to lineation; and form another, weaker maximum that is parallel lineation and within the plane of foliation. [010] axes form a girdle with a concentration of measurements perpendicular to foliation and perpendicular to lineation. [001] axes are coincident with the plane of foliation and form one diffuse maximum parallel to lineation, and another diffuse maximum perpendicular to lineation. With reference to the geographic reference frame, one of the double maxima of the [100] axes is identical to the orientation of [100] axes in the Central Domain fabric (the EW, horizontal axes). Consequently, we interpret that a typical Central Domain LPO fabric once existed in these rocks, and that this relict LPO fabric was only partially overprinted by the younger, shear-related fabrics in the South-dipping Domain.

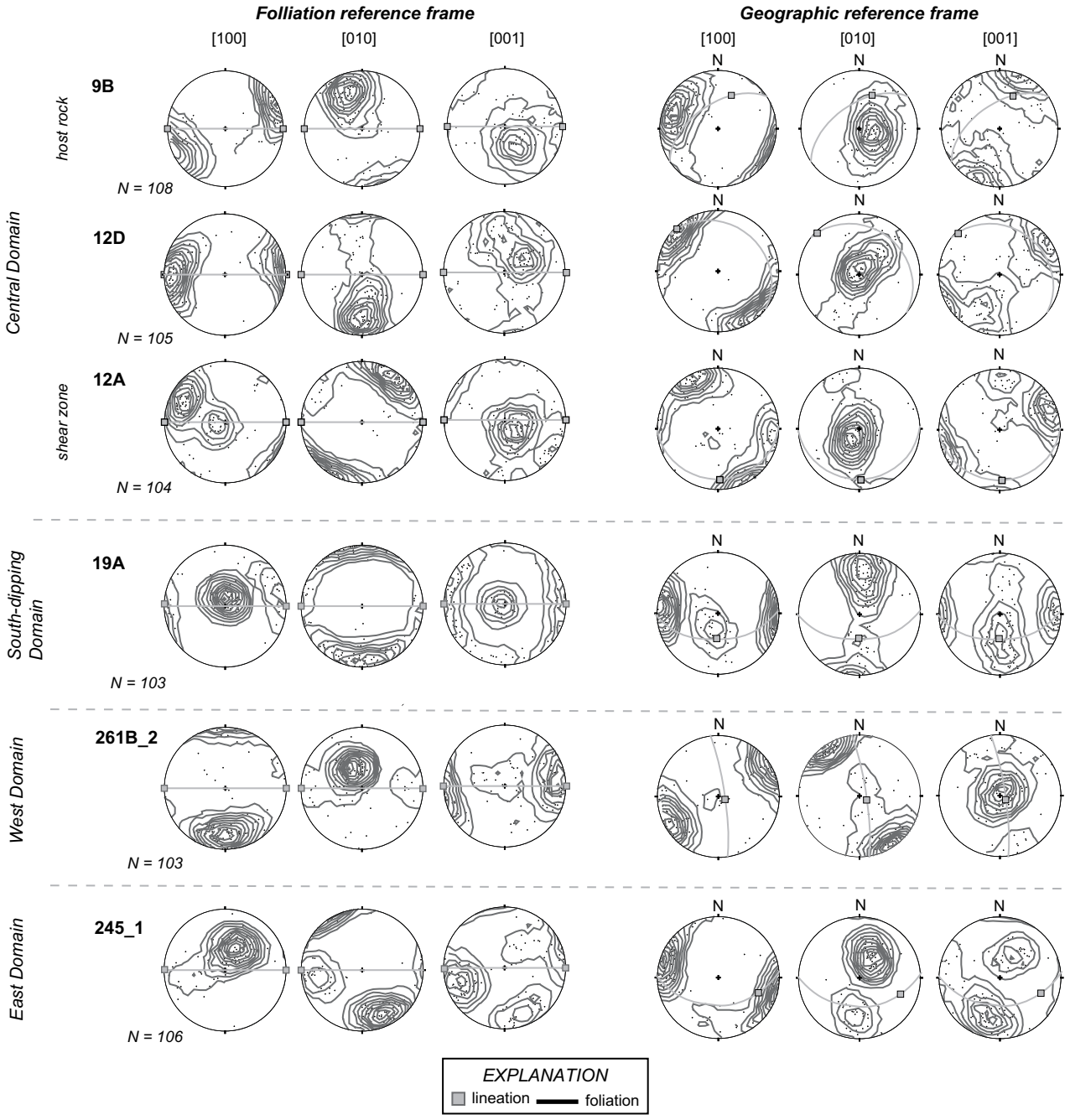

Fig. 8. Lower hemisphere equal area nets of olivine LPO in the different structural domains. Data are contoured at an interval of 2σ using the method described by Kamb (1959). Data on the right-hand side were rotated such that foliation is oriented E–W and vertical, and lineation is horizontal in the plane of foliation (sample-specific reference frame). Data on the left-hand side were plotted in real coordinate space, with North on the top of the stereonet (geographic reference frame). In the geographic reference frame, the line represents the field foliation plane and the box is the field lineation. See text for description of LPO.

Measurements of olivine LPO in the West Domain record a maximum of [100] axes perpendicular to foliation and perpendicular to lineation. The [010] axes are coincident with the plane of foliation and are concentrated in a maximum perpendicular to lineation, and the [001] axes are coincident with the plane of foliation and form a maximum parallel to lineation. Multiple samples from the West Domain show strong point maxima LPO, unlike the double maximum observed for the small-scale shear zones and South-dipping Domain. Consequently, we interpret that the pre-existing fabric of the Central Domain was completely reset by subsequent deformation in the West Domain.

Olivine LPO in a sample from the East Domain yields a pattern similar to that measured in the sample from the South-dipping Domain, but is less symmetrical. This sample contains a maximum of [100] axes sub-parallel to compositional foliation and perpendicular to lineation. The [010] axes are concentrated in two maxima; a strong maximum is oriented $\sim 30^{\circ}$ from perpendicular to foliation, and a weak maximum is oriented sub-parallel to lineation in the plane of foliation. The [001] axes form two weak double maxima that are in similar orientations to the maxima of [010] axes. A concentration of [001] axes is located sub-parallel to foliation and lineation, and another concentration of [001] axes is located $\sim 30^{\circ}$

from perpendicular to foliation. The geographic reference frame is, once again, critical for interpretation of the data. The [100] axes are identical in the Central Domain and East Domain. The [010] axes in the East domain are parallel to the local lineation or, most generally, parallel to the orientation of [010] axes in the Central Domain. Again, the LPO data provides clear evidence that the Central Domain fabric pre-existed and was overprinting by fabrics in the East Domain.

In summary, the LPO data for the South-dipping and East Domains show a clear evidence for incorporation of a pre-existing LPO from the Central Domain. In contrast, the point maximum of the West Domain has no spatial relation to the Central Domain LPO, indicating that complete overprinting took place in this zone.

7. Mineral chemistry

7.1. Analytical techniques

Mineral phases were analyzed using a Cameca SX51 electron probe microanalyzer (EMPA) with Probe for Windows software at the Eugene Cameron Microprobe Lab at the University of Wisconsin-Madison. Operating conditions consisted of an accelerating voltage of 15 kV and a beam current of 15 nA (pyroxene) and 20 nA (olivine and spinel). Counting times varied from 10 s for major elements and up to 30 s for minor elements to improve counting statistics.

We analyzed two or three areas from each thin section that contained adjacent orthopyroxene, clinopyroxene, olivine, and spinel (Table 1). We collected $\geq$3 points in the center of each olivine and spinel grain using a 1 μm beam diameter. Pyroxene grains typically contained very thin (<5 μm) exsolution lamellae, and in order to determine the compositions of these grains prior to exsolution, we analyzed 5–47 points per grain (depending on grain size) using a defocused electron beam (50 μm).

7.2. Geothermometry

We estimated temperatures using the Taylor (1998) and Brey and Kohler (1990) formulations of the two-pyroxene geothermometer. We estimated pressure using a five-phase assemblage present in a clinopyroxenite dike deformed in a small-scale, south-dipping zone in the Central Domain (outcrop RH04-15). The dike contains an assemblage common to many rocks in the field area, including: clinopyroxene, orthopyroxene, olivine, spinel and plagioclase. This is a stable pyroxenite composition at ~7–8 kbar and temperatures of ~850–950 °C (Fig. 10 and Fig. 12 in Schmadicke, 2000). It should be noted we have very little constraint on the pressure; however, the effect of pressure on the temperature calculations is minor. A change of 5 kbar in pressure effects a change of ~15 °C in the temperature obtained from the Taylor (1998) equation, and effects a change of ~10 °C in the Brey and Kohler (1990) two-pyroxene equation.

7.3. Results: temperature of deformation at Red Hills

We obtained temperature estimates from two or three areas per thin section from two samples of Central Domain host rock (samples 24 and 54), two samples from small-scale shear zones in the Central Domain (samples 15J and 22A1), and one sample each from the South-dipping Domain (sample 19A), West Domain (sample 32B), and East Domain (sample 82). Additionally, we obtained a temperature from one olivine websterite dike (15J_2). The results are reported in Table 1 and shown in Fig. 9.

Preliminary application of the two-pyroxene geothermometers yields temperatures ranging from 750 to 1050 °C, with most results between 850 and 950 °C. Calculated temperatures vary among different locations in a structural domain as well as among different areas of a single thin section. For example, samples 24 and 54 from the Central Domain yield temperatures ranging from 870 to 1025 °C. Two areas from the same thin section in sample 54 yield temperatures that differ by >100 °C (890 and 1025 °C). Similarly, in a shear zone, three areas from within the same thin section yield temperatures that range from 769 to 952 °C. A discussion of uncertainty in geothermometry calculations is presented in Webber (2005).

The variability in temperature on the scale of a thin section suggests deformation events in the Red Hills occurred at different temperatures, and there has been a variable and incomplete resetting of compositions between these events. In some samples, microstructural differences are consistent with the estimated temperature variations. For example, in the East Domain, the temperature estimated from pyroxenes varies within a thin section (sample 82). Smaller, recrystallized pyroxene grains that are in contact with plagioclase yield lower temperatures than coarser pyroxene grains. This result suggests that younger deformation produced the grains that yield lower temperatures. Given the uncertainties, some caution is required in interpreting these results. However, the agreement within domains (e.g., East Domain) and the difference between domains (e.g., East Domain vs. West Domain) suggest that some preliminary interpretations are possible.

8. Discussion: overprinting in the upper mantle

8.1. Timing of structural overprinting of the Central Domain

We interpret that the Central Domain contains the oldest foliation in the Red Hills field area, based on observed cross-cutting and overprinting field relationships. The Central Domain was overprinted by the South-dipping, West, and East Domains as discussed in the following section and illustrated in Fig. 10.

The South-dipping Domain is interpreted to be a ~50-m-thick shear zone that overprints the Central Domain (Fig. 10B). Field relationships indicate a progressive change in foliation at the contact between the Central and South-dipping Domains. Cross-cutting relationships indicate that a shear-related compositional foliation formed in the South-dipping Domain after formation of the Central Domain. However, compositional foliation in the South-dipping Domain formed before or during the deformation that produced offset on small-scale south-dipping shear zones found in both the Central and South-dipping Domains.

The West Domain is interpreted to be a shear zone that overprints and transposes the older fabrics in the Central and South-dipping Domains (Fig. 10C). The interpretation is based on progressive folding and transposition of the older, Central Domain compositional banding across the contact between Central and West Domains. Additionally, we observe north-dipping compositional foliation, presumably that of the Central Domain, preserved locally in apparent low-strain enclaves in the West Domain. We interpret these field relations to indicate that the Central Domain fabric once existed throughout the West Domain, but is presently only preserved in low-strain lozenges within a high-strain domain. Further supporting evidence for this sequence of overprinting is the absence of any south-dipping shear zones in the West Domain. We note, however, that the contact between West Domain and South-dipping Domain is poorly exposed.

The East Domain is interpreted to be the youngest structural domain in the field area (Fig. 10D). The East Domain exhibits microstructures that are distinct from the other structural domains, such as core-and-mantle structure and interlobate grain boundaries. Such microstructures form at lower temperatures (or higher strain rates) than the polygonal textures that characterize the other

Table 1
Data used in in geothermometry calculations

Sample	Central Domain 24_1				Central Domain 24_2				Central Domain 24_3				Central Domain 54_2			
Phase	opx	cpx	ol	sp	opx	cpx	ol	sp	opx	cpx	ol	sp	opx	cpx	ol	sp
Wt% oxides: all Fe as FeO; 5 to 47 measurements averaged for pyroxene, 2 to 9 measurements averaged for spinel and olivine																
SiO_2	53.98	50.50	40.54	0.00	54.18	50.57	41.05	0.00	54.63	51.34	40.83	0.00	54.28	51.77	40.55	0.00
TiO_2	0.03	0.07	0.00	0.05	0.03	0.10	0.00	0.04	0.03	0.08	0.00	0.03	0.04	0.12	0.00	0.08
Al_2O_3	2.85	3.67	0.00	38.84	2.97	3.78	0.00	39.37	3.19	3.62	0.00	40.08	2.72	3.13	0.00	35.47
Cr_2O_3	0.61	1.05	0.00	27.97	0.66	1.17	0.00	28.03	0.69	1.06	0.00	26.75	0.61	0.96	0.00	30.84
V_2O_3	0.00	0.00	0.00	0.16	0.00	0.00	0.00	0.14	0.00	0.00	0.00	0.15	0.00	0.00	0.00	0.21
FeO	6.24	2.60	9.28	15.82	6.20	3.03	8.88	15.84	6.22	2.46	8.92	16.33	6.35	2.39	9.28	7.11
MnO	0.16	0.10	0.12	0.15	0.16	0.10	0.13	0.17	0.15	0.09	0.16	0.16	0.16	0.09	0.14	0.14
MgO	33.21	16.95	48.84	15.62	33.11	16.70	49.15	15.39	32.91	16.74	49.44	15.48	33.07	16.97	49.06	14.94
CaO	0.97	22.62	0.01	0.00	1.08	22.43	0.02	0.00	1.18	22.98	0.01	0.00	0.89	22.85	0.00	0.00
ZnO	0.00	0.00	0.00	0.18	0.00	0.00	0.00	0.27	0.00	0.00	0.00	0.30	0.00	0.00	0.00	0.23
NiO	20.00	0.00	0.38	0.00	0.00	0.00	0.37	0.00	0.00	0.00	0.39	0.00	0.00	0.00	0.36	0.00
Na_2O	0.0	0.24	0.00	0.00	0.01	0.24	0.00	0.00	0.02	0.21	0.00	0.00	0.01	0.19	0.00	0.00
Total	98.06	97.80	99.17	98.78	98.39	98.12	99.60	99.24	99.01	98.57	99.75	99.28	98.12	98.46	99.39	99.02
Atomic units: Olivine and spinel calculated on the basis of four oxygens; orthopyroxene calculated on the basis of six oxygens																
Si	0.91	1.88	1.00	0.00	1.91	1.88	1.01	0.00	1.91	1.90	1.00	0.00	1.92	1.91	1.00	0.00
Ti	0.00	0.00	0.00	0.00	0.00	0.00	0.00	0.00	0.00	0.00	0.00	0.00	0.00	0.00	0.00	0.00
Al	0.12	0.16	0.00	1.32	0.12	0.17	0.00	1.33	0.13	0.16	0.00	1.35	0.11	0.14	0.00	1.22
Cr	0.02	0.03	0.00	0.64	0.02	0.03	0.00	0.64	0.02	.03	0.00	0.60	0.02	0.03	0.00	0.71
V	0.00	0.00	0.00	0.00	0.00	0.00	0.00	0.00	0.00	0.00	0.00	0.00	0.00	0.00	0.00	0.00
Fe	0.18	0.08	0.19	0.38	0.18	0.09	0.18	0.38	0.18	0.08	0.18	0.39	0.19	0.07	0.19	0.42
Mn	0.00	0.00	0.00	0.00	0.00	0.00	0.00	0.00	0.00	0.00	0.00	0.00	0.00	0.00	0.00	0.00
Mg	1.75	0.94	1.80	0.67	1.74	0.93	1.80	0.66	1.72	0.92	0.81	0.66	1.74	0.93	1.80	0.65
Ca	0.04	0.90	0.00	0.00	0.04	0.89	0.00	0.00	0.04	0.91	0.00	0.00	0.03	0.90	0.00	0.00
Zn	0.00	0.00	0.00	0.00	0.00	0.00	0.00	0.01	0.00	0.00	0.00	0.01	0.00	0.00	0.00	0.01
Ni	0.00	0.00	0.01	0.00	0.00	0.00	0.01	0.00	0.00	0.00	0.01	0.00	0.00	0.00	0.01	0.00
Na	0.00	0.02	0.00	0.00	0.00	0.02	0.00	0.00	0.00	0.02	0.00	0.00	0.00	0.01	0.00	0.00
Total	4.02	4.03	3.00	3.02	4.02	4.02	2.99	3.02	4.01	4.01	3.00	3.02	4.02	4.01	3.00	303
Calculated temperatures: Ca-2 px (1) from Taylor (1998); Ca-2 px (2) from Brey and Kohler (1990)																
Ca-2 px (1)	876				904				871				889			
Ca-2 px (2)	905				933				884				889			

Sample	Central Domain 54_3				Central Domain 15J_2				Central Domain 15J_1				Central Domain 22A1_1			
Phase	opx	cpx	ol	sp	opx	cpx	ol	sp	opx	cpx	ol	sp	opx	cpx	ol	sp
Wt% oxides: all Fe as FeO; 5 to 47 measurements averaged for pyroxene, 2 to 9 measurements averaged for spinel and olivine																
SiO_2	54.28	51.15	40.53	0.00	54.51	51.40	40.72	0.00	54.73	50.48	40.80	0.00	54.77	51.83	40.88	0.00
TiO_2	0.03	0.09	0.00	0.08	0.04	0.11	0.00	0.04	0.06	0.14	0.00	0.09	0.03	0.07	0.00	0.12
Al_2O_3	2.21	3.56	0.00	32.12	2.76	4.02	0.00	38.57	2.66	3.74	0.00	31.34	1.58	1.76	0.00	21.68
Cr_2O_3	0.62	1.11	0.00	33.51	0.60	1.11	0.00	27.32	0.69	1.16	0.00	35.29	0.54	0.73	0.00	44.23
V_2O_3	0.00	0.00	0.00	0.26	0.00	0.00	0.00	0.15	0.00	0.00	0.00	0.21	0.00	0.00	0.00	0.33
FeO	6.44	2.89	9.29	19.36	6.39	2.89	9.48	17.65	6.32	2.65	9.52	18.93	6.21	2.27	9.40	21.53
MnO	0.16	0.09	0.14	0.17	0.16	0.09	0.14	0.17	0.14	0.10	0.16	0.21	0.16	0.08	0.14	0.21
MgO	32.94	17.57	48.64	13.42	33.13	17.31	49.21	14.74	32.94	16.92	49.32	13.21	32.94	17.31	49.26	11.05
CaO	0.95	21.65	0.02	0.00	0.89	21.69	0.01	0.00	1.19	22.44	0.00	0.00	1.60	23.77	0.01	0.00
ZnO	0.00	0.00	0.00	0.32	0.00	0.00	0.00	0.33	0.00	0.00	0.00	0.25	0.00	0.00	0.00	0.19
NiO	0.00	0.00	0.41	0.00	0.00	0.00	0.38	0.00	0.00	0.00	0.44	0.00	0.00	0.00	0.39	0.00
Na_2O	0.01	0.19	0.00	0.00	0.01	0.26	0.00	0.00	0.01	0.28	0.00	0.00	0.01	0.07	0.00	0.00
Total	97.64	98.29	99.05	99.22	98.50	98.89	99.93	98.98	98.75	97.91	100.26	99.54	97.85	97.89	100.08	99.35
Atomic units: Olivine and spinel calculated on the basis of four oxygens; orthopyroxene calculated on the basis of six oxygens																
Si	1.93	1.89	1.00	0.00	1.92	1.89	1.00	0.00	1.92	1.88	1.00	0.00	1.94	1.93	1.00	0.00
Ti	0.00	0.00	0.00	0.00	0.00	0.00	0.00	0.00	0.00	0.00	0.00	0.00	0.00	0.00	0.00	0.00
Al	0.09	0.16	0.00	1.13	0.11	0.17	0.00	1.32	0.11	0.16	0.00	1.11	0.07	0.08	0.00	0.81
Cr	0.02	0.03	0.00	0.79	0.02	0.03	0.00	0.63	0.02	0.03	0.00	0.84	0.02	0.02	0.00	1.11
V	0.00	0.00	0.00	0.01	0.00	0.00	0.00	0.00	0.00	0.00	0.00	0.01	0.00	0.00	0.00	0.01
Fe	0.19	0.09	0.19	0.48	0.19	0.09	0.19	0.43	0.19	0.08	0.19	0.47	0.18	0.07	0.19	0.57
Mn	0.00	0.00	0.00	0.00	0.00	0.00	0.00	0.00	0.00	0.00	0.00	0.01	0.00	0.00	0.00	0.01
Mg	1.74	0.97	1.79	0.60	1.74	0.95	1.80	0.64	1.72	0.94	1.80	0.59	1.74	0.96	1.80	0.52
Ca	0.04	0.86	0.00	0.00	0.03	0.85	0.00	0.00	0.04	0.90	0.00	0.00	0.06	0.95	0.00	0.00
Zn	0.00	0.00	0.00	0.01	0.00	0.00	0.00	0.01	0.00	0.00	0.00	0.01	0.00	0.00	0.00	0.00
Ni	0.00	0.00	0.01	0.00	0.00	0.00	0.01	0.00	0.00	0.00	0.01	0.00	0.00	0.00	0.01	0.00
Na	0.00	0.01	0.00	0.00	0.00	0.02	0.00	0.00	0.00	0.02	0.00	0.00	0.00	0.00	0.00	0.00
Total	4.02	4.02	3.00	3.03	4.02	4.01	3.00	3.03	4.01	4.03	3.00	3.02	4.02	4.02	3.00	3.03
Calculated temperatures: Ca-2px (1) from Taylor (1998); Ca-2 px (2) from Brey and Kohler (1990)																
Ca-2 px (1)	998				999				891				745			
Ca-2 px (2)	1025				1023				923				769			

Sample	Central Domain 22A1_2				Central Domain 22A1_3				Central Domain 19A_1				Central Domain 32B_1			
Phase	opx	cpx	ol	sp	opx	cpx	ol	sp	opx	cpx	ol	sp	opx	cpx	ol	sp
Wt% oxides: all Fe as FeO; 5 to 47 measurements averaged for pyroxene, 2 to 9 measurements averaged for spinel and olivine																
SiO_2	53.54	51.48	40.87	0.00	54.66	52.23	40.83	0.00	43.02	50.87	40.59	0.00	54.56	51.46	40.67	0.00
TiO_2	0.03	0.08	0.00	0.14	0.03	0.07	0.00	0.14	0.04	0.12	0.00	0.09	0.03	0.07	0.00	0.07

Table 1 (*continued*)

Sample	Central Domain 22A1_2				Central Domain 22A1_3				Central Domain 19A_1				Central Domain 32B_1			
Phase	opx	cpx	ol	sp	opx	cpx	ol	sp	opx	cpx	ol	sp	opx	cpx	ol	sp
Al_2O_3	1.41	1.38	0.00	20.98	1.48	1.73	0.00	24.68	2.02	3.27	0.00	29.16	2.72	3.20	0.00	36.13
Cr_2O_3	0.42	0.38	0.00	44.21	0.52	0.83	0.00	40.15	0.71	1.27	0.00	36.74	0.67	1.07	0.00	31.01
V_2O_3	0.00	0.00	0.00	0.25	0.00	0.00	0.00	0.32	0.00	0.00	0.00	0.23	0.00	0.00	0.00	0.17
FeO	6.48	2.40	9.43	22.48	5.90	2.30	9.41	23.65	5.49	2.14	8.80	19.08	6.28	2.62	9.37	17.61
MnO	0.16	0.09	0.14	0.25	0.16	0.08	0.13	0.27	0.16	0.06	0.12	0.20	0.16	0.11	0.15	0.17
MgO	33.75	18.42	49.10	10.47	32.47	17.41	49.07	10.18	30.27	16.72	49.20	13.21	32.19	16.68	49.09	14.44
CaO	0.82	22.26	0.01	0.00	2.21	23.90	0.01	0.00	1.25	22.68	0.01	0.00	1.77	22.46	0.02	0.00
ZnO	0.00	0.00	0.00	0.25	0.00	0.00	0.00	0.36	0.00	0.00	0.00	0.19	0.00	0.00	0.00	0.30
NiO	0.00	0.00	0.34	0.00	0.00	0.00	0.40	0.00	0.00	0.00	0.43	0.00	0.00	0.00	0.35	0.00
Na_2O	0.00	0.09	0.00	0.00	0.02	0.10	0.00	0.00	0.02	0.39	0.00	0.00	0.02	0.22	0.00	0.00
Total	96.62	96.57	99.89	99.05	97.45	98.64	99.85	99.76	82.97	97.51	99.15	98.90	98.41	97.89	99.66	99.90
Atomic units: Olivine and spinel calculated on the basis of four oxygens; orthopyroxene calculated on the basis of six oxygens																
Si	1.93	1.94	1.00	0.00	1.95	1.93	1.00	0.00	1.82	1.90	1.00	0.00	1.92	1.91	1.00	0.00
Ti	0.00	0.00	0.00	0.00	0.00	0.00	0.00	0.00	0.00	0.00	0.00	0.00	0.00	0.00	0.00	0.00
Al	0.06	0.06	0.00	0.79	0.06	0.08	0.00	0.91	0.10	0.14	0.00	1.05	0.11	0.14	0.00	1.24
Cr	0.01	0.01	0.00	1.12	0.01	0.02	0.00	1.00	0.02	0.04	0.00	0.88	0.02	0.03	0.00	0.71
V	0.00	0.00	0.00	0.01	0.00	0.00	0.00	0.01	0.00	0.00	0.00	0.01	0.00	0.00	0.00	0.00
Fe	0.19	0.08	0.19	0.60	0.18	0.07	0.19	0.62	0.19	0.07	0.18	0.49	0.19	0.08	0.19	0.43
Mn	0.00	0.00	0.00	0.01	0.00	0.00	0.00	0.01	0.01	0.00	0.00	0.01	0.00	0.00	0.00	0.00
Mg	1.81	1.03	1.79	0.50	1.72	0.96	1.79	0.48	1.91	0.93	1.81	0.60	1.69	0.92	1.80	0.63
Ca	0.03	0.90	0.00	0.00	0.08	0.95	0.00	0.00	0.06	0.91	0.00	0.00	0.07	0.89	0.00	0.00
Zn	0.00	0.00	0.00	0.01	0.00	0.00	0.00	0.01	0.00	0.00	0.00	0.00	0.00	0.00	0.00	0.01
Ni	0.00	0.00	0.01	0.00	0.00	0.00	0.01	0.00	0.00	0.00	0.01	0.00	0.00	0.00	0.01	0.00
Na	0.00	0.01	0.00	0.00	0.00	0.01	0.00	0.00	0.00	0.03	0.00	0.00	0.00	0.02	0.00	0.00
Total	4.04	4.03	3.00	3.04	4.01	4.02	3.00	3.04	4.12	4.02	3.00	3.03	4.01	4.01	3.00	3.02
Calculated temperatures: Ca-2px (1) from Taylor (1998); Ca 2-px (2) from Brey and Kohler (1990)																
Ca-2 px (1)	927				749				828				918			
Ca-2 px (2)	952				777				857				926			

Sample	Central Domain 32B_2				Central Domain 82_1				Central Domain 82_2				Central Domain 82_3			
Phase	opx	cpx	ol	sp	opx	cpx	ol	sp	opx	cpx	ol	sp	opx	cpx	ol	sp
Wt% oxides: all Fe as FeO; 5 to 47 measurements averaged for pyroxene, 2 to 9 measurements averaged for spinel and olivine																
SiO_2	54.60	52.24	40.47	0.00	54.61	52.41	40.38	0.00	54.37	51.61	40.36	0.00	54.58	50.31	40.26	0.00
TiO_2	0.03	0.08	0.00	0.02	0.04	0.11	0.00	0.09	0.04	0.11	0.00	0.07	0.04	0.11	0.00	0.04
Al_2O_3	2.65	3.24	0.00	37.26	2.56	2.79	0.00	31.49	3.23	3.51	0.00	39.68	3.31	3.80	0.00	40.32
Cr_2O_3	0.62	0.99	0.00	31.11	0.67	1.01	0.00	35.54	0.67	0.99	0.00	26.82	0.67	1.13	0.00	26.48
V_2O_3	0.00	0.00	0.00	0.14	0.00	0.00	0.00	0.18	0.00	0.00	0.00	0.18	0.00	0.00	0.00	0.14
FeO	6.37	2.58	9.59	15.90	6.35	2.24	9.26	17.82	6.06	2.47	8.88	16.49	6.23	2.49	9.37	16.33
MnO	0.17	0.10	0.16	0.13	0.16	0.08	0.16	0.16	0.14	0.09	0.15	0.16	0.14	0.09	0.14	0.15
MgO	2.37	16.89	48.72	15.23	32.74	16.76	48.80	13.68	31.95	16.59	49.16	15.51	32.40	16.68	48.57	15.39
CaO	1.16	22.70	0.01	0.00	1.13	23.39	0.02	0.00	1.96	22.90	0.02	0.00	1.46	22.91	0.01	0.00
ZnO	0.00	0.00	0.00	0.32	0.00	0.00	0.00	0.19	0.00	0.00	0.00	0.20	0.00	0.00	0.00	0.21
NiO	0.00	0.00	0.37	0.00	0.00	0.00	0.36	0.00	0.00	0.00	0.40	0.00	0.00	0.00	0.36	0.00
Na_2O	0.01	0.23	0.00	0.00	0.03	0.24	0.00	0.00	0.03	0.18	0.00	0.00	0.02	0.18	0.00	0.00
Total	97.98	99.05	99.31	100.10	98.29	99.03	98.98	99.16	98.46	98.44	98.97	99.12	98.84	97.70	98.71	99.05
Atomic units: Olivine and spinel calculated on the basis of four oxygens; orthopyroxene calculated on the basis of six oxygens																
Si	1.93	1.92	1.00	0.00	1.93	1.93	1.00	0.00	1.92	1.91	1.00	0.00	1.91	1.88	1.00	0.00
Ti	0.00	0.00	0.00	0.00	0.00	0.00	0.00	0.00	0.00	0.00	0.00	0.00	0.00	0.00	0.00	0.00
Al	0.11	0.14	0.00	1.26	0.11	0.12	0.00	1.11	0.13	0.15	0.00	1.34	0.14	0.17	0.00	1.36
Cr	0.02	0.03	0.00	0.71	0.02	0.03	0.00	0.84	0.02	0.03	0.00	0.61	0.02	0.03	0.00	0.60
V	0.00	0.00	0.00	0.00	0.00	0.00	0.00	0.00	0.00	0.00	0.00	0.00	0.00	0.00	0.00	0.00
Fe	0.19	0.08	0.20	0.38	0.19	0.07	0.19	0.45	0.18	0.08	0.18	0.40	0.18	0.08	0.19	0.39
Mn	0.01	0.00	0.00	0.00	0.00	0.00	0.00	0.00	0.00	0.00	0.00	0.00	0.00	0.00	0.00	0.00
Mg	1.71	0.92	1.79	0.65	1.72	0.92	1.80	0.61	1.68	0.91	1.81	0.66	1.69	0.93	1.80	0.66
Ca	0.04	0.89	0.00	0.00	0.04	0.92	0.00	0.00	0.07	0.91	0.00	0.00	0.05	0.92	0.00	0.00
Zn	0.00	0.00	0.00	0.01	0.00	0.00	0.00	0.00	0.00	0.00	0.00	0.00	0.00	0.00	0.00	0.00
Ni	0.00	0.00	0.01	0.00	0.00	0.00	0.01	0.00	0.00	0.00	0.01	0.00	0.00	0.00	0.01	0.00
Na	0.00	0.02	0.00	0.00	0.00	0.02	0.00	0.00	0.00	0.01	0.00	0.00	0.00	0.01	0.00	0.00
Total	4.00	4.00	3.00	3.01	4.01	4.01	3.00	3.02	4.01	4.00	3.00	3.02	4.01	4.02	3.00	3.02
Calculated temperatures: Ca-2px (1) from Taylor (1998); Ca-2px (2) from Brey and Kohler (1990)																
Ca-2 px (1)	922				822				900				853			
Ca-2 px (2)	932				826				904				874			

structural domains. This interpretation is consistent with geothermometry results that indicate lower temperatures in the East Domain. Thus, the microstructural observations and geothermometry results suggest that deformation in the East Domain is later, and therefore overprints the higher temperature deformation of the other domains. Furthermore, we observe transitions in foliation characteristics at the contact between the Central and East Domains consistent with overprinting.

One curious result from the study is the lack of significant grain size variation among the Central, South-dipping, and West Domains (the East Domain exhibits smaller grain size). We suspect that post-deformational annealing is the cause for this pattern,

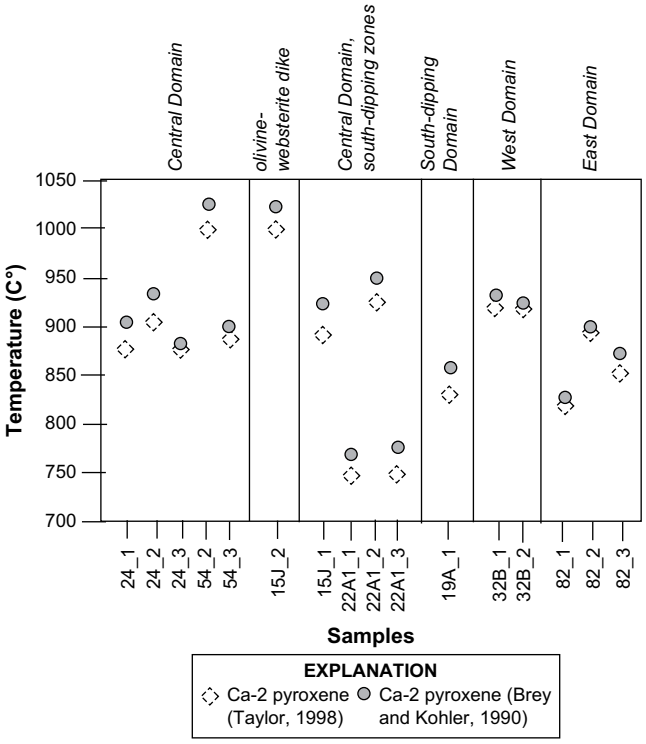

Fig. 9. Geothermometry results from structural domains in the Red Hills.

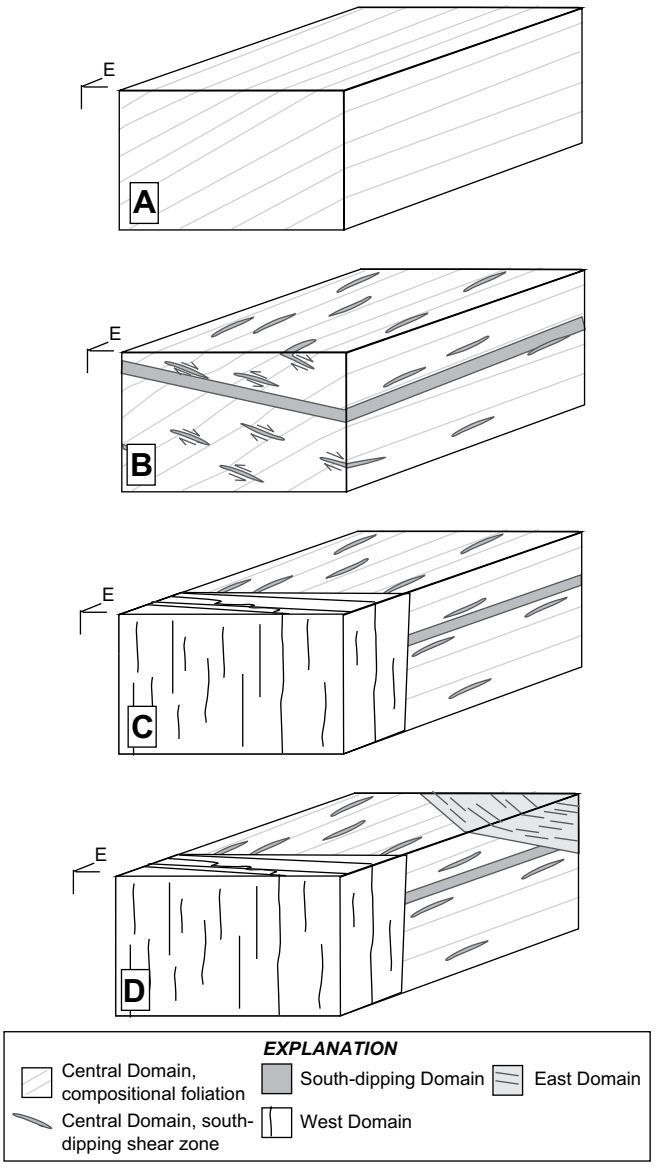

Fig. 10. Block diagrams illustrating history of deformation in Red Hills field area. (A) Formation of Central Domain north-dipping compositional foliation (grey lines), which are locally preserved in the central portion of the field area. (B) Formation of cm-scale south-dipping shear zones that cross-cut compositional foliation, and formation of South-dipping Domain. (C) Formation of the West Domain, transposing earlier Central Domain and South-dipping Domain fabrics. (D) Formation of the East Domain, transposing the Central and South-dipping Domain fabrics.

which might result in a larger grain size without resetting the LPO. If so, this interpretation does not allow us to use paleopiezometers based on recrystallized grain size for olivine-rich rocks (Van der Wal et al., 1993). This interpretation, however, appears at odds with the relatively low temperatures determined by 2-pyroxene thermometers. This issue requires further work for a satisfactory resolution.

In summary, we interpret the following sequence of events. (1) Central Domain foliation is formed everywhere in the Red Hills. (2) South-dipping Domain and south-dipping shear zones in the Central Domain form. (3) West Domain foliation is transposed on the western side of Porter's Knob. (4) East Domain foliation is transposed on the eastern side of Porter's Knob. The key difference between this interpretation and an earlier interpretation of large-scale folding (Walcott, 1965) is that we attribute the changes in foliation orientation to fabric transposition events that were spatially localized into discrete high-strain zones (probably shear zones). The result of these superpositions is an intersecting mosaic of overprinting, diachronous fabrics. Fabric dips are, as a consequence, spatially variable; and the deformation is heterogeneous at the km-scale. Although large-scale folding of a widespread, regionally contemporaneous fabric may exist elsewhere in the Red Hills, folding is not consistent with our field observations, microstructural analysis, or thermometry of the area around Porter's Knob.

8.2. Evidence for overprinting relationships from olivine LPO and geothermometry

Comparison of olivine LPO data from the Central, South-dipping, East, and West domains leads to two main interpretations. First, only the samples from the Central Domain host rock show exclusively the high-temperature slip system (010)[100], although it is the most common slip system predicted on the basis of experimental studies to form in the upper mantle (Kohlstedt and Goetze, 1974; Durham and Goetze, 1977; Mercier, 1985; Bai et al., 1991; Bai and Kohlstedt, 1992; Hanson and Spetzler, 1994). The South-dipping Domain also records the activity of the slip system (010)[100], but the co-existing, diffuse lineation-parallel maximum of [001] axes also suggests activity of the lower-temperature slip system (010)[001].

Second, olivine LPOs in the West and East Domains also show concentrations of [001] axes parallel to lineation. These suggest slip on the system (010)[001] (Nicolas and Poirier, 1976). Recent workers have observed similar olivine LPO in peridotite deformed in the presence of water (Jung and Karato, 2001; Frese et al., 2003; Mizukami et al., 2004) or in the presence of melt (Holtzman, 2003). However, we do not observe microstructures like those reported in other deformed water-bearing peridotites (Mizukami et al., 2004) or in deformed melt-bearing peridotites (Holtzman, 2003). See Webber (2005) for a complete discussion of the olivine LPO patterns.

The variable olivine LPO patterns are consistent with a wide range of temperatures calculated by geothermometry. Thus, it is possible that an original high-temperature LPO, which is preserved in the host rock of the Central Domain, was variably overprinted in the other domains during younger, lower-temperature deformation events. This interpretation is also consistent with double maxima observed in the South-dipping and East Domains; the implications of this hypothesis and the amount of finite strain required to reset an LPO are explicitly explored in a companion study (Webber et al., submitted for publication).

8.3. Significance of overprinting in the upper mantle at Red Hills

Overprinting relationships identified at Red Hills make this massif seemingly unique among other upper mantle peridotites. The similarity in microstructures among different structural domains (Central, South-dipping, and West Domains) suggests that the overprinting history was restricted to a range of temperatures and pressures in the upper mantle. The similarities in microstructures we observe at Red Hills are different than observed in shear zones from other upper mantle peridotites. The observed fabrics do not fit neatly into the "asthenospheric" vs. "lithospheric" framework for mantle deformation utilized in other studies of ultramafic rocks formed in spreading centers (Ceuleneer et al., 1988; Suhr, 1992). Well-studied peridotites (e.g., Oman ophiolite, Rhonda massif, Erro-Tobbio massif) commonly contain shear zones; but their activity is typically attributed to final uplift and emplacement of the massifs (Dijkstra et al., 2004 and references therein). For example, Hoogerduijn Strating et al. (1993) report five generations of shear zones in the Erro-Tobbio peridotite, a slice of subcontinental mantle in the Voltri massif. The different structures are interpreted to have formed at different temperature and pressure conditions associated with rifting and development of the Piemonte-Ligurian Oceanic Basin. Cook et al. (2000) report exhumation-related mylonitic shear zones in the Lizard peridotite massif and emplacement related structures. Van der Wal and Vissers (1993) and Vissers et al. (1997) also report mylonites in peridotite related to emplacement.

Structural domains and overprinting relationships at Red Hills are also different from similar features described by Suhr (1992). Suhr (1992) identified six structural domains and overprinted fabrics in the Bay of Islands ophiolite, and related the fabrics to mid-ocean ridge processes and obduction. Structural domains are primarily distinguished on the basis of lineation orientation, but the orientation of foliation is similar everywhere in the study area (Suhr, 1992). Furthermore, Suhr (1992) interprets that the structural domains occurred at different pressure and temperature conditions based on differences in microstructures in each domain. These deformation characteristics are different than at Red Hills, where the orientation of foliation is distinctly different in each structural domain and microstructures (except for East Domain) are similar.

Within the Red Hills ultramafic complex, the spatial variation in fabric expression and transposition, changes in fabric attitudes, and the variable and complex LPO patterns of these rocks suggests that discrete deformational (probably shearing) events superposed one another at lithospheric mantle conditions across a range of temperatures. Given the relatively uncertain tectonic setting for the Red Hills ultramafic complex – partly resulting from the lack of an associated crustal section – interpretation of the tectonic significance would be highly speculative. The clear result, however, is that overprinting patterns can occur in the lithospheric mantle and that the deformation of these rocks can be markedly heterogeneous at the kilometer-scale.

9. Conclusions

We identified two main results from a combined study of field mapping, geothermometry, and olivine LPO in the Red Hills massif.

(1) *Variable overprinting of deformational fabrics that occurred in the upper mantle is preserved at Red Hills.* We identified four structural domains (Central, South-dipping, East, and West Domains) in the Red Hills field area. The Central Domain's older compositional banding was overprinted in the South-dipping domain and transposed in the West and East domains by inferred large-scale shear zones. High-temperature microstructures, characterized by coarse, polygonal grains that are indicative of high-temperature deformation or fast recovery, are preserved in the Central, South-dipping, and West Domains. The Central Domain preserves LPOs indicative of the high-temperature (010)[100] slip system, whereas, the South-dipping, West, and East Domains contain a mixture of lower-temperature LPO patterns that are interpreted to record a variable ductile overprinting of the original compositional banding. The East Domain contains distinctive core-and-mantle microstructures that are consistent with this structural domain being a later, lower temperature (or higher strain rate) fabric. Temperatures calculated by geothermometry are variable, which is consistent with an interpretation of variable overprinting.

(2) *The upper mantle, preserved in the Red Hills, records a history of spatially heterogeneous deformation.* We identify at least three structural domains that overprinted an earlier foliation in the Central Domain. The four preserved structural domains suggest that the upper mantle may be subject to a complex deformational history, and thus acquire a heterogeneous deformational fabric, especially when viewed at the kilometer-scale. The possibility of multiple overprinting fabrics in the upper mantle may be more common that currently considered for upper mantle deformation.

Acknowledgements

We thank John Fournelle, director of the Eugene Cameron Microprobe Lab at the University of Wisconsin-Madison, for his assistance in EPMA data collection. Thanks to Bryn Benford, JoAnn Gage, Angela Hull, Carrie Larsen for their assistance in collecting olivine LPO data. Peter J. Berquist was a helpful field assistant at Red Hills. Special thanks to Eric Horsman for early reconnaissance work at Porter's Knob. We appreciate the helpful insights on mantle petrology from Gordon Medaris. We acknowledge that financial support for this project was provided by NSF EAR-0409522 and by the Packard Foundation.

References

Bai, Q., Kohlstedt, D.L., 1992. High-temperature creep of olivine single crystals: 2. Dislocation structures. Tectonophysics 206, 1–29.

Bai, Q., Mackwell, S.J., Kohlstedt, D.L., 1991. High-temperature creep of olivine single crystals: 1. Mechanical results for buffered samples. Journal of Geophysical Research 96, 2441–2463.

Brey, G.P., Kohler, T., 1990. Geothermobarometry in four-phase lherzolites II. New thermobarometers, and practical assessment of existing thermobarometers. Journal of Petrology 31, 1353–1378.

Ceuleneer, D., Nicolas, A., Boudier, F., 1988. Mantle flow patterns at an oceanic spreading centre: the Oman peridotites record. Tectonophysics 151, 1–26.

Challis, G.A., 1965. High-temperature contact metamorphism at the Red Hills Ultramafic Intrusion – Wairau Valley – New Zealand. Journal of Petrology 6, 395–419.

Christensen, N.I., 1984. The magnitude, symmetry and origin of upper mantle anisotropy based on analyses of ultramafic tectonites. Geophysical Journal of the Royal Astronomical Society 76, 89–111.

Coombs, D.S., Landis, C.A., Norris, R.J., Sinton, J.M., Borns, D.J., Craw, D., 1976. The Dun Mountain Ophiolite Belt, New Zealand, its tectonic setting, constitution, and origin, with special reference to the southern portion. American Journal of Science 276, 561–603.

Cook, C.A., Holdsworth, R.E., Styles, M.T., Pearce, J.A., 2000. Pre-emplacement structural history recorded by mantle peridotites: an example from the Lizard Complex, SW England. Journal of the Geological Society (London, U.K.) 157, 1049–1064.

Cooper, A.F., Barriero, B.A., Kimbrough, D.L., Mattinson, J.M., 1987. Lamprophyre dike intrusion and the age of the Alpine fault, New Zealand. Geology 5, 941–944.

Davis, T.E., Johnston, M.R., Rankin, P.C., Stull, R.J., 1980. The Dun Mountain Ophiolite Belt in East Nelson, New Zealand. In: Proceedings, International Ophiolite Symposium. Cyprus Ministry of Agriculture and Natural Resources, Nichoisa, Cyprus, pp. 480–498.

Dijkstra, A.H., Drury, M.R., Vissers, R.L.M., Newman, J., Van Roermund, H.L.M., 2004. In: Alsop, G.I., Holdsworth, R.E., McCaffrey, K.J.W., Hand, M. (Eds.), Shear zones in the upper mantle: evidence from alpine- and ophiolite-type peridotite massifs. Flow Processes in Faults and Shear Zones. Geological Society Special Publications, London, pp. 11–24.

Durham, W.B., Goetze, C., 1977. Plastic flow of oriented single crystals of olivine. Journal of Geophysical Research 82, 5737–5753.

Frese, K., Trommsdorff, V., Kunze, K., 2003. Olivine [100] normal to foliation: lattice preferred orientation in prograde garnet peridotite formed at high H_2O activity, Cim di Gagnone (Central Alps). Contributions to Mineralogy and Petrology 145, 75–86.

Hanson, D.R., Spetzler, H.A., 1994. Transient creep in natural and synthetic, iron-bearing olivine single crystals: mechanical results and dislocation microstructures. Tectonophysics 235, 293–315.

Holtzman, B.K., Kohlstedt, D.L., Zimmerman, M.E., Heidelbach, F., Hiraga, T., Hustoft, J., 2003. Melt segregation and strain partitioning: implications for seismic anisotropy and mantle flow. Science 301, 1227–1230.

Hoogerduijn Strating, E.H., Rampone, E., Piccardo, G.B., Drury, M.R., Vissers, R.L.M., 1993. Subsolidus emplacement of mantle peridotites during incipient oceanic rifting and opening of the Mesozoic Tethys (Voltri Massif, NW Italy). Journal of Petrology 34, 901–927.

Johnston, M.R., 1986. Dun Mountain Ophiolite and the Permian–Mesozoic rocks of East Nelson. In: Houghton, B.F., Weaver, S.D. (Eds.), South Island Igneous Rocks; Tour Guides A3, C2, and C7. New Zealand Geological Survey, Lower Hutt, New Zealand, pp. 5–37.

Johnston, M.R., 1982. Geological Map of New Zealand. New Zealand Geological Survey, scale 1:50,000.

Jung, H., Karato, S., 2001. Water-induced fabric transitions in olivine. Science 293, 1460–1463.

Kamb, W.B., 1959. Ice petrofabric observations from Blue Glacier, Washington, in relation to theory and experiment. Journal of Geophysical Research 64, 1891–1909.

Kimborough, D.L., Mattison, J.M., Coombs, D.S., Landis, C.A., Johnston, M.R., 1992. Uranium-lead ages from the Dun Mountain Ophiolite Belt and Brook Street Terrane, South Island, New Zealand. Geological Society of America Bulletin 104, 429–443.

Kohlstedt, D.L., Goetze, C., 1974. Low-stress high-temperature creep in olivine single crystals. Journal of Geophysical Research 79, 2045–2051.

Malahoff, A., 1965. Gravity and Geological Studies of an Ultramafic Massif in New Zealand. M.S. thesis, Hawaii Institute of Geophysics.

Mercier, J.-C.C., 1985. Olivine and pyroxenes. In: Wenk, H.R. (Ed.), Preferred Orientation in Deformed Metals and Rocks: an Introduction to Modern Texture Analysis. Academic Press, Orlando, pp. 407–430.

Mercier, J.-C.C., Nicolas, A., 1975. Textures and fabrics of upper-mantle peridotites as illustrated by xenoliths from basalts. Journal of Petrology 16, 454–487.

Michibayashi, K., Mainprice, D., 2004. The role of pre-existing mechanical anisotropy on shear zone development within oceanic mantle lithosphere; an example from the Oman Ophiolite. Journal of Petrology 45, 405–414.

Mizukami, T., Wallis, S.R., Yamamoto, J., 2004. Natural examples of olivine lattice preferred orientation patterns with a flow-normal *a*-axis maximum. Nature 427, 432–436.

Nicolas, A., Poirier, J.P., 1976. Crystalline Plasticity and Solid State Flow in Metamorphic Rocks. John Wiley and Sons, London.

Paterson, M.S., 2001. Relating experimental and geological rheology. International Journal of Earth Science 90, 157–167.

Sano, S., Tazaki, K., Koide, Y., Nagao, T., Watanabe, T., Kawachi, Y., 1997. Geochemistry of dike rocks in Dun Mountain Ophiolite, Nelson, New Zealand. New Zealand Journal of Geology and Geophysics 40, 127–136.

Savage, M.K., 2002. Seismic anisotropy and mantle deformation in the western United States and southwestern Canada. International Geology Review 44, 913–937.

Schmadicke, E., 2000. Phase relations in peridotitic and pyroxenitic rocks in the model systems CMASH and NCMASH. Journal of Petrology 41, 69–85.

Sivell, W.J., McCulloch, M.T., 2000. Reassessment of the origin of the Dun Mountain Ophiolite, New Zealand: Nd-isotopic and geochemical evolution of magma suites. New Zealand Journal of Geology and Geophysics 43, 133–146.

Suhr, G., 1992. Upper mantle peritotites in the Bay of Islands Ophiolite, Newfoundland: formation during the final stages of a spreading center. Tectonophysics 206, 31–53.

Sutherland, R., 1995. The Australia–Pacific boundary and Cenozoic plate motions in the SW Pacific: some constraints from Geosat data. Tectonics 14, 819–831.

Taylor, W.R., 1998. An experimental test of some geothermometer and geobarometer formulations for upper mantle peridotites with application to the thermobarometry of fertile lherzolite and garnet websterite. Neues Jahrbuch fuer Mineralogie 178, 381–408.

Van der Wal, D., Chopra, P., Drury, M., Fitz Gerald, J., 1993. Relationships between dynamically recrystallised grain size and deformation conditions in experimentally deformed olivine rocks. Geophysical Research Letters 20, 1479–1482.

Van der Wal, D., Vissers, R.L.M., 1993. Uplift and emplacement of upper mantle rocks in the western Mediterranean. Geology 21, 1119–1122.

Vissers, R.L.M., Drury, M.R., Newman, J., Fliervoet, T.F., 1997. Mylonitic deformation in upper mantle peridotites of the North Pyrenean Zone (France): implications for strength and strain localization in the lithosphere. Tectonophysics 297, 303–325.

Walcott, R.I., 1969. Geology of the Red Hill Complex, Nelson, New Zealand. Transactions of the Royal Society of New Zealand 7, 57–88.

Walcott, R.I., 1965. Structure and Petrology of the Red Hill Complex, Nelson. PhD thesis, Victoria University of Wellington.

Webber, C.E. 2005. Structural Geology of the Porter's Knob Area, Red Hills Ultramafic Massif, New Zealand: Implications for Upper Mantle Deformation. MS thesis. University of Wisconsin-Madison.

Webber, C.E., Newman, J., Holyoke, C., Little, T., Tikoff, B. Fabric development in cm-scale shear zones in ultramafic rocks, Red Hills, New Zealand. Tectonophysics, submitted for publication.

Wendt, A.S., Mainprice, D., Rutter, E., Wirth, R., 1998. A joint study of experimental deformation and experimentally induced microstructures of pretextured peridotites. Journal of Geophysical Research 103, 18205–18221.